Discovery of Selective Estrogen Receptor Covalent Antagonists (SERCAs) for the Treatment of ERα^{WT} and ERα^{MUT} Breast Cancer

Xiaoling Puyang[1]*, Craig Furman[1]*, Guo Zhu Zheng[1]*, Zhenhua J. Wu[1], Deepti Banka[1], Kiran Aithal[2], Sergei Agoulnik[3], David M. Bolduc[1], Silvia Buonamici[1], Benjamin Caleb[1], Subhasree Das[1], Sean Eckley[3], Peter Fekkes[1], Ming-Hong Hao[1], Andrew Hart[3], René Houtman[4], Sean Irwin[1], Jaya J. Joshi[1], Craig Karr[1], Amy Kim[1], Namita Kumar[3], Pavan Kumar[1], Galina Kuznetsov[3], Weidong G. Lai[3], Nicholas Larsen[1], Crystal Mackenzie[1], Lesley-Ann Martin[5], Diana Melchers[4], Alyssa Moriarty[6], Tuong-Vi Nguyen[1], John Norris[7], Morgan O'Shea[1], Sunil Pancholi[5], Sudeep Prajapati[1], Sujatha Rajagopalan[2], Dominic J. Reynolds[1], Victoria Rimkunas[1], Nathalie Rioux[1], Ricardo Ribas[5], Amy Siu[3], Sasirekha Sivakumar[2], Vanitha Subramanian[1], Michael Thomas[1], Frédéric H. Vaillancourt[1], John Wang[1], Suzanne Wardell[7], Michael J. Wick[6], Shihua Yao[1], Lihua Yu[1], Markus Warmuth[1], Peter G. Smith[1], Ping Zhu[1#] and Manav Korpal[1#]

[1]H3 Biomedicine, Inc., 300 Technology Square, Cambridge, MA 02139, USA.
[2]Aurigene Discovery Technologies Ltd, #39-40 (P), KIADB Industrial Area, Electronic City Phase II, Hosur Road, Bangalore, Karnataka, 560100, India.
[3]Eisai Inc., 4 Corporate Drive, Andover, MA 01810, USA.
[4]PamGene International, Wolvenhoek 10, 5211HH Den Bosch, The Netherlands.
[5]The Breast Cancer Now, Toby Robins Research Centre, The Institute of Cancer Research, London, SW7 3RP.
[6]START, Preclinical Research, San Antonio, TX 78229.
[7]Duke University, Research Drive, LSRC Bldg, C251, Durham, NC 27710, USA.

* These authors contributed equally

Running title: Selective Estrogen Receptor Covalent Antagonists for Treatment of Breast Cancer.

Corresponding authors: Manav Korpal, H3 Biomedicine, Inc., 300 Technology Square, Cambridge, MA 02139. E-mail: Manav_Korpal@h3biomedicine.com; and Ping Zhu, Ping_Zhu@h3biomedicine.com.

COMPETING FINANCIAL INTERESTS: X.P., C.F., G.Z.Z., Z.J.W., D.B., S.A., D.M.B., S.B., B.C., S.D., S.E., P.F., M-H.H., A.H., S.I., J.J.J., C.K., A.K., N.K., P.K., G.K., W.G.L., N.L., C.M., T-V.N., M.O., S.P., D.J.R., V.R., N.R., A.S., V.S., M.T., F.H.V., J.W., S.Y., L.Y., M.W., P.G.S., P.Z., and M.K are present or past employees of H3 Biomedicine, Inc. and Eisai Inc. The remaining authors declare no competing financial interests.

Abstract

Mutations in estrogen receptor alpha (ERα) that confer resistance to existing classes of endocrine therapies are detected in up to 30% of patients who have relapsed during endocrine treatments. Since a significant proportion of therapy-resistant breast cancer metastases continue to be dependent on ERα signaling, there remains a critical need to develop the next generation of ERα antagonists that can overcome aberrant ERα activity. Through our drug discovery efforts, we identified H3B-5942 which covalently inactivates both wild-type and mutant ERα by targeting Cys530 and enforcing a unique antagonist conformation. H3B-5942 belongs to a class of ERα antagonist referred to as Selective Estrogen Receptor Covalent Antagonists (SERCAs). *In vitro* comparisons of H3B-5942 with standard of care (SoC) and experimental agents confirmed increased antagonist activity across a panel of $ERα^{WT}$ and $ERα^{MUT}$ cell lines. *In vivo*, H3B-5942 demonstrated significant single-agent antitumor activity in xenograft models representing $ERα^{WT}$ and $ERα^{Y537S}$ breast cancer that was superior to fulvestrant. Lastly, H3B-5942 potency can be further improved in combination with CDK4/6 or mTOR inhibitors in both $ERα^{WT}$ and $ERα^{MUT}$ cell lines and/or tumor models. In summary, H3B-5942 belongs to a class of orally available ERα covalent antagonists with an improved profile over SoCs.

Significance

Nearly 30% of endocrine-therapy resistant breast cancer metastases harbor constitutively activating mutations in ERα. Selective Estrogen Receptor Covalent Antagonist (SERCA) H3B-5942 engages C530 of both $ER\alpha^{WT}$ and $ER\alpha^{MUT}$, promotes a unique antagonist conformation, and demonstrates improved *in vitro* and *in vivo* activity over standard of care (SoC) agents. Importantly, single agent efficacy can be further enhanced by combining with CDK4/6 or mTOR inhibitors.

Introduction

Breast cancer is the second leading cause of cancer mortality among women worldwide with more than 1 million new cases diagnosed each year and approximately 400,000 deaths annually [1]. Nearly 70% of breast cancers express estrogen receptor alpha (ERα), a key hormone-regulated transcription factor for normal and malignant breast cells. Nonclinical and clinical-epidemiological studies highlight an important oncogenic role for ERα in the genesis and progression of breast cancer [2]. Several ER-directed therapies have been developed to antagonize oncogenic ERα function including selective ER modulators (SERM; tamoxifen), selective ER downregulators (SERD; fulvestrant), selective nonsteroidal aromatase inhibitors (NSAI; anastrozole and letrozole), and steroidal aromatase inhibitors (exemestane) [3], for use in women with locally advanced, recurrent or metastatic cancer. Although these therapies have demonstrated antitumor efficacy in the clinic, innate and acquired resistance remains a major challenge. Several mechanisms of resistance to endocrine therapies have been identified including: "crosstalk" between ERα and other kinases, particularly HER2 [4], dysregulation of apoptosis- and cell cycle-related regulators [5], aberrant expression of ERα coactivators/corepressors [6] and most recently, recurrent mutations in ERα ($ERα^{MUT}$) [7–9]. The hotspot mutations in ERα, which are enriched in nearly 30% of endocrine therapy-resistant metastases, induce ligand-independent activation of the ERα pathway [7-12], confer partial resistance to existing classes of endocrine therapies, and are associated with more aggressive disease biology with shorter overall survival in patients relative to the wild-type *ESR1* [13]. Since current endocrine therapies are only partially effective in the ERα mutant setting, and a significant proportion of endocrine-therapy resistant metastases continue to remain dependent on ERα signaling for growth/survival, there remains a critical need to develop the next generation

of ERα antagonists that can overcome aberrant activities of both wild-type ($ER\alpha^{WT}$) and $ER\alpha^{MUT}$.

Herein, we report the discovery of a covalent class of ERα antagonist referred to as Selective Estrogen Receptor Covalent Antagonist (SERCA) that inactivates both $ER\alpha^{WT}$ and $ER\alpha^{MUT}$ by targeting a unique cysteine residue (C530) that is not conserved among the other steroid hormone receptors. H3B-5942 enforces a unique antagonist conformation in ERα and demonstrates increased ERα antagonism compared to standard of care (SoC) therapies in preclinical models. We further show that the activity of H3B-5942 can be improved in combination with CDK4/6 or mTOR inhibitors suggesting a potential combination strategy for SERCAs in the clinical setting.

Results

Identification of H3B-5942

It has previously been shown that hotspot ERα mutations identified in endocrine refractory metastatic breast cancer promote constitutive activity in ERα [7-12]. Consistent with previous reports, we also noted estradiol (E2)-independent ERα activity conferred by the hotspot mutations Y537S/C/N and D538G (Supplementary Fig. S1A-B). Among the hotspot mutations, the Y537S mutant demonstrated the greatest E2-independent reporter activity (Supplementary Fig. S1A-B). To further assess the functional role of ERα mutations in promoting resistance to currently marketed endocrine therapies, the $ER\alpha^{WT}$ positive MCF7 breast cancer line was engineered to ectopically express ERα hotspot variants (Fig. 1A). Consistent with earlier data (Supplementary Fig. 1A-B), ectopic expression of $ER\alpha^{Y537S}$ or $ER\alpha^{D538G}$ constitutively activated ERα function as determined by an increased E2-independent expression of ERα target genes

GREB1 and *TFF1* (Supplementary Fig. S1C). In regular culture medium (10% FBS), treatment with ERα antagonists raloxifene or fulvestrant led to a reduction in ERα pathway activity in control cells (Vector and $ERα^{WT}$) whereas higher pathway activity persisted in $ERα^{Y537S}$ and $ERα^{D538G}$ expressing cells (Fig. 1B; Supplementary Fig. S1D). Importantly, enhanced pathway activity in mutant ERα expressing lines was associated with partial resistance to the anti-proliferative effects of 4-hydroxytamoxifen (4-OHT) and fulvestrant (Fig. 1C), confirming the functional role of ERα mutations as drivers of partial resistance to SoC endocrine therapies. Of note was the observation that the most constitutively activating mutation Y537S was also associated with the greatest resistance phenotype following 4-OHT treatment (Fig. 1C). In summary, ERα mutations constitutively activate ERα function and promote partial resistance to anti-estrogen therapies.

Mechanistically, the Y537 and D538 mutations are located in the AF-2 helix of ERα and introduce a stabilizing interaction to shift the dynamic equilibrium towards the agonist conformation even in the absence of ligand [14, 15]. We reasoned that for a compound to be more active in the mutant setting, it would necessarily have to overcome the stabilizing effects of the mutation and shift the equilibrium towards the destabilized antagonist conformation. In principle, manipulating this dynamic equilibrium could be achieved through enhancing the compound potency against the receptor, either through covalent or non-covalent interactions, or a combination of both, in a primary or allosteric binding site. By targeting a non-conserved cysteine at the 530 position at the end of helix H11 that presents in the ligand-binding pocket of ERα when the receptor is in the antagonist conformation (Fig. 1D), our drug discovery efforts ultimately led to the identification of H3B-5942 (Fig. 1E).

H3B-5942 was confirmed to engage covalently with ERα by intact mass spectrometry with >95% covalent modification observed for $ERα^{WT}$ and $ERα^{Y537S}$ ligand-binding domains (LBDs) after overnight incubation at 4°C (Fig. 1F). To confirm C530 as the site of modification, intact mass spectrometry was performed with $ERα^{WT}$ and $ERα^{Y537S}$ LBDs harboring a cysteine to serine substitution at position 530 ($ERα^{C530S}$, and $ERα^{C530S,Y537S}$, respectively). As expected, H3B-5942 was found to specifically engage with C530 as no covalent adduct was detected for ERα harboring the C530S mutation and the abundance of unmodified proteins was equal to that observed for DMSO controls (Fig. 1F).

To further confirm covalent engagement at C530 and to better understand the structural impact of H3B-5942 binding on ERα conformation, we determined the co-crystal structure of $ERα^{Y537S}$ bound to H3B-5942 at 1.89 Å resolution (PDB ID 6CHW; Supplementary Table S1) (Fig. 1G). The continuous electron density between C530 and the Michael acceptor confirmed covalent engagement. Moreover, the crystal structure shows the receptor adopts the desired antagonist conformation in the mutant setting. The indazole core is anchored at the bottom of the pocket through an H-bond to E353, while the flexible linker extends upwards from the core to C530. An internal H-bond within the linker side chain helps orient the Michael acceptor with respect to the cysteine. Overall, these data confirm H3B-5942 as an ERα-targeting small molecule that specifically engages the C530 residue covalently to enforce the antagonist conformation.

H3B-5942 is a member of a covalent class of ERα antagonist with unique profiles

To profile the impact of covalent engagement on cellular ERα protein, we first performed Western blot analysis for ERα in the $ERα^{WT}$ expressing MCF7 parental line and the $ERα^{Y537S/WT}$

expressing ST941 PDX-derived cell line (PDX-ERα$^{Y537S/WT}$) (Supplementary Fig. S2), following a 24 hour treatment with fulvestrant, 4-OHT, or H3B-5942. In contrast to fulvestrant, which degraded ERα, H3B-5942 and 4-OHT treatments showed no alteration (MCF7 parental cell line) to slight elevation (ST941 cell line) in ERα protein levels, suggesting that the latter two compounds may maintain the pool of ERα in the antagonist conformation (Fig. 2A).

Next, we evaluated the influence of SERCA binding on the conformational change of ERα in cells. It is well accepted that conformational changes of ERα in response to ligand binding can have a significant impact on its biological function through influencing sites that are ultimately accessible for coregulator binding [16, 17]. We applied a mammalian 2-hybrid based reporter assay with a panel of nuclear receptor coactivators and conformationally sensitive peptides to evaluate their ability to interact with H3B-5942-bound ERα [18–20] (Fig. 2B; Supplementary Fig. S3; Supplementary Table S2). Compared to wild-type ERα, endocrine-resistant ERα^{Y537S} and ERα^{D538G} demonstrated a remarkably higher interaction with LXXLL-containing coactivators/peptides in the absence of E2, suggesting that the constitutive activity of mutant ERα is likely mediated by ligand-independent recruitment of coactivators (Supplementary Fig. S3). All of the ERα antagonists tested at 10 μM, including H3B-5942, substantially reduced binding of these LXXLL-containing peptides to both ERα^{WT} and ERα ^{MUT} (Supplementary Fig. S3). A noteworthy observation was that while SERMs and SERDs induced interactions between ERα^{WT} and the conformational peptides specific for the corresponding antagonists [17], the H3B-5942-ERα complex did not recruit any of the tested peptides, indicating that H3B-5942 induces a distinct conformation in ERα (Fig. 2B). Similarly, H3B-5942-bound ERα^{Y537S} and ERα^{D538G} also failed to interact with conformationally sensitive

peptides that are specifically recruited by the SERM- or SERD-bound mutant ERα (Fig. 2B), further confirming a potentially unique conformational alteration induced by H3B-5942 that would represent a novel antagonistic mechanism for both wild-type and mutant ERα. Since it is well appreciated that the conformation of ERα is an essential determinant of its biological activity, these results imply that H3B-5942 may impart some divergent responses in ERα relative to SoC and other agents in the SERD/SERM class.

To interrogate the potential transcriptional impact of H3B-5942, we investigated its influence on genome-wide DNA-binding modes of ERα in MCF7 cells using chromatin immunoprecipitation followed by high-throughput DNA sequencing (ChIP-Seq). This analysis revealed that the peak overlap of global ERα binding sites was highly consistent across different compound treatments, including E2, 4-OHT, fulvestrant and H3B-5942 (Supplementary Fig. S4A). The read distribution correlation analysis indicated that the ERα binding profile of H3B-5942 treatment was more related to that of 4-OHT treatment (Supplementary Fig. S4B). Moreover, motif enrichment analysis revealed that the classic estrogen response elements (ERE) AGGTCA-N(3)-TGACCT was the top binding consensus for H3B-5942 (Supplementary Fig. S4C). Together, these data suggest that H3B-5942 induces a similar global DNA-binding pattern as other ERα ligands.

Next, we explored the gene expression profiles of H3B-5942 relative to SoCs under E2 containing (antagonist mode) and E2-depleted (agonist mode) conditions. RNA-seq analysis of parental MCF7 breast cancer cells cultured in media supplemented with FBS and treated with various compounds for 6 days revealed a large subset of genes commonly suppressed by all compounds, enriched for pathways involved in cell cycle and estrogen signaling (Supplementary Fig. S5, Supplementary Tables S3, and S4). Interestingly, whereas fulvestrant, regulated the

expression of a number of unique genes not affected by other treatments, H3B-5942 treatment induced gene expression changes more similar to 4-OHT under these conditions (Supplementary Fig. S5A, B). These data indicate that H3B-5942, similar to the SERDs/SERMs profiled, can potently suppress ERα-dependent transcription in breast cancer cells.

As a SERM, 4-OHT can stimulate ERα signaling under certain contexts, such as in the absence of estradiol, in the normal uterus and the Ishikawa endometrial carcinoma line [21]. To assess for potential SERM activity of H3B-5942 in the uterine tissue, H3B-5942 was dosed once daily for three days at 10, 30 and 100 mg/kg in postnatal day (PND) 19 Sprague-Dawley rat pups. In agreement with the global transcriptional studies above, H3B-5942 was comparable to SERM tamoxifen as both compounds similarly increased the absolute (data not shown) and relative (to body weight) uterine weights, and enhanced endometrial epithelium thickness (Supplementary Fig. S6).

Having demonstrated SERM activity of H3B-5942 in the normal uterus, we next aimed to investigate H3B-5942 activity in the endometrial carcinoma setting. As expected, 4-OHT was able to induce ERα activity in Ishikawa carcinoma cells noted by the significant increase in *PGR* expression and enhanced proliferation (Fig. 2C-E). Consistent with its role as a pure antagonist, treatment with fulvestrant significantly suppressed *PGR* expression at all concentrations. Interestingly, although fulvestrant did not induce proliferation at low concentrations, it did have a stimulatory effect at 300 nM, perhaps due to induction of non-genomic pathways (Fig. 2C-E). In contrast to 4-OHT, H3B-5942 did not robustly affect *PGR* expression or induce proliferation of Ishikawa cells at any concentration tested (Fig. 2C-E). In summary, these data suggest that although H3B-5942 shares features of SERMs, unique context-dependent functions are also observed, possibly driven by the unique ERα conformation induced upon H3B-5942 binding.

H3B-5942 is dependent on covalent engagement for enhanced ERα antagonism

We next aimed to define the role covalent engagement plays in influencing ERα antagonist activity. To enable these studies, we synthesized the saturated analog of H3B-5942, denoted here as H3B-9224, which lacks the electrophilic Michael acceptor (Fig. 3A). Comparison of the co-crystal structure of ERα^{Y537S}-H3B-9224 (PDB ID 6CHZ; Supplementary Table S1) with H3B-5942 shows similar binding modes for the pharmacophore and similar conformations for Helix-12. However, the linker conformations appear to diverge, showing a higher degree of flexibility in that part of H3B-9224. In contrast to H3B-5942, a potential interaction between the secondary amine group of H3B-9224 and ERα-D351 was observed, similar to the conventional SERMs such as 4-OHT (PDB ID 3ERT) and raloxifene (PDB ID 1ERR) (Fig. 3A).

We next questioned whether the different linker conformations for H3B-5942 and H3B-9224 would impact residence time on ERα and, eventually, downstream antagonist activity. Given that we previously showed highly selective engagement of ERα C530 by H3B-5942 (Fig. 1F), ERα proteins containing the C381S and C417S double mutation were used for further kinetic characterization as they showed greater stability allowing detailed *in vitro* characterization [22, 23]. The K_d values of estradiol for ERα^{WT} and ERα^{Y537S} were determined to be 0.144 and 0.030 nM, respectively, suggesting a 5-fold higher affinity of ERα^{Y537S} for estradiol (Supplementary Fig. S7A). These values are in agreement with a recent study [24] but are significantly lower than values published in previous studies [14, 25], likely due to differences in experimental design. Based on the precise determination of the affinity for estradiol, we determined that the K_i value for non-covalent H3B-9224 was ~2-fold higher than 4-OHT for ERα^{WT} and ERα^{Y537S} (Supplementary Fig. S7B).

To estimate the residence time of various ERα binding compounds, jump dilution experiments were performed using initially saturating concentrations of binders. An excess of ^{3}H-estradiol was then used to titrate the number of ERα sites that were no longer bound to the initial binder after dilution. This experiment demonstrated that H3B-9224 and 4-OHT were competed off ERα^{WT} and ERα^{Y537S} similarly, while H3B-5942 was essentially irreversibly bound due to the covalent nature of its interaction (Fig. 3B). Thus, the longer residence time of H3B-5942 could conceivably play a role in its antagonistic activity towards wild-type and mutant ERα.

Having confirmed the irreversible binding of H3B-5942, we next examined the functional relevance of covalent engagement on ERα conformation, protein abundance, and transcriptional activity. Interestingly, H3B-9224 binding to ERα also induced a novel conformation relative to known ERα-ligand complexes using conformationally sensitive peptides (Supplementary Table S2, Supplementary Fig. S8A). However, it is unclear whether different conformational states in ERα may be induced between H3B-5942 and H3B-9224 since conformation-specific probes are currently not available for either of these ERα-ligand complexes. Importantly, although H3B-9224 did not influence overall ERα abundance in cells (Supplementary Fig. S8B), weaker cellular activity was noted (Fig. 3C, D). Gene expression analysis of two independent ERα target genes *GREB1* and *TFF1* consistently showed reduced potency of H3B-9224 relative to H3B-5942 across both ERα^{WT} and ERα^{MUT} lines (Fig. 3C). Consistent with the gene expression analysis, H3B-9224 also showed weaker anti-proliferative activity across ERα^{WT} and ERα^{MUT} lines, confirming the biological importance of covalent engagement for ERα antagonism (Fig. 3D). These data suggest that the increase in potency observed for H3B-5942 in the cellular setting is driven, at least in part, by covalent binding.

To further confirm the functional importance of covalency, we performed proliferation assays in MCF7 lines engineered to express ERα^{WT} or ERα^{Y537S} with C530S point mutations (Fig. 3D; Supplementary Fig. S8C). The C530S point mutation in ERα^{WT} (ERα^{C530S}) did not hinder basal or estradiol-mediated ERα activity (Supplementary Fig. S8D). Proliferation assays demonstrated that the C530S mutation in ERα conferred reduced activity to H3B-5942 but not H3B-9224 (Fig. 3D; Supplementary Fig. S9), reinforcing the observation that H3B-5942 activity is critically dependent on covalent engagement with C530 for ERα antagonism in breast cancer lines, a phenotype that may be potentially driven by a combination of unique conformation (Fig. 2B) and enhanced residence time on ERα (Fig. 3B).

Since we previously confirmed that H3B-5942 demonstrates weaker agonism relative to 4-OHT in Ishikawa endometrial carcinoma cells (Fig. 2C-E), we next aimed to profile ERα agonism induced by H3B-9224 relative to H3B-5942. H3B-9224 demonstrated modestly higher agonistic activity relative to H3B-5942 as assessed by expression analysis of a subset of E2 regulated genes, including *PGR* (Supplementary Fig. S10A, B). Collectively, these data imply that covalent engagement with C530 may enhance ERα antagonism while concomitantly tuning down agonist activity in carcinoma cells.

H3B-5942 potently suppresses ERα function and demonstrates potent anti-proliferative activity in a panel of ERα^{WT} and ERα^{MUT} lines

Having demonstrated a significant potency gain for H3B-5942 through covalent engagement, we next aimed to assess the antagonist potential of H3B-5942 relative to SoC and experimental agents in breast cancer models. H3B-5942 showed a high apparent affinity for both ERα^{WT} and ERβ^{WT} comparable to SoCs and GDC-0810 (Supplementary Fig. S11A). To study

the impact of high-affinity ERα binding on coregulator recruitment, we extended our previous analysis (Supplementary Fig. S3) to assess coregulator interactions globally using two independent methods (Supplementary Fig. S11B, C). FRET-based analysis revealed an 1) increase in CoA peptide recruitment to $ER\alpha^{WT}$ following E2 treatment relative to the apo form, 2) higher basal recruitment of CoAs to $ER\alpha^{Y537S}$ relative to $ER\alpha^{WT}$ in the absence of ligand supporting the constitutive activity observed for $ER\alpha^{MUT}$, and 3) H3B-5942 broadly suppresses CoA recruitment with little impact on CoR interaction (Supplementary Fig. S11B). As further validation of the FRET-based coregulator interaction profiling, we screened WT ER co-regulator interactions using the Microarray Assay for Real-time Co-regulator-Nuclear receptor Interaction [26]. These data support the TR-FRET analysis (Supplementary Fig. S11C), confirming that H3B-5942, in these settings, primarily prevents CoA recruitment with minimal influence on CoR interactions.

To quantitatively determine the impact of various treatments on CoA recruitment, an enzyme-fragment complementation-based cellular assay was performed to measure the interaction of ERα with the CoA PGC1α. Although all treatments significantly suppressed recruitment of PGC1α, H3B-5942 was superior to both 4-OHT and GDC-0810 (Supplementary Fig. S11A). This potent inhibition in the recruitment of PGC1α was selective to $ER\alpha^{WT}$ as recruitment to other steroid hormone receptors was not significantly impacted by H3B-5942 (Supplementary Fig. S11A).

As recruitment of CoAs to ERα is a prerequisite for ERα activity, we hypothesized that the potent inhibition in CoA recruitment by H3B-5942 would lead to enhanced suppression in cellular ERα signaling, comparable or superior to existing classes of ERα antagonists. Indeed,

H3B-5942 showed a significant dose-dependent suppression of the ERα target gene *GREB1* in MCF7-ERα^{WT}, various MCF7–ERα^{MUT} lines, and the PDX-ERα$^{Y537S/WT}$ line, which was superior to that observed for 4-OHT and GDC-0810 (Fig. 4A). Consistent with the transcriptional profile, H3B-5942 also exhibited a dose-dependent reduction in proliferation superior to 4-OHT and GDC-0810 (Fig. 4B).

We next further characterized H3B-5942 in the endocrine-therapy resistant setting in MCF7 cells resistant to long-term-estrogen-deprivation (LTED), which express either ERα^{WT} (MCF7-LTED-ERα^{WT}) or spontaneously gained the ERα^{Y537C} mutation (MCF7-LTED-ERα^{Y537C}) [27]. In the absence of E2, H3B-5942 showed no significant impact on ER-mediated transcription in the MCF7-Parental (endocrine-therapy sensitive) and MCF7-LTED-ERα^{Y537C} lines but did result in a 1.5-fold (p=0.03) increase in the MCF7-LTED-ERα^{WT} line. In contrast, 4-OHT showed no significant impact on ER-mediated transcription in all cell lines tested, whereas fulvestrant caused a 30% reduction in both MCF7-Parental and MCF7-LTED-ERα^{WT} lines (Supplementary Fig. S12). In the presence of E2, H3B-5942 showed a significant dose-dependent decrease in ER-mediated transactivation in all cell lines tested, comparable to fulvestrant and superior to 4-OHT (Supplementary Fig. S12). Consistent with this reduction in ER activity, H3B-5942 caused a concentration-dependent decrease in proliferation in all cell lines tested with GI_{50}s of 0.5, 2 and 30 nM in the MCF7-Parental, MCF7-LTED-ERα^{WT}, and MCF7-LTED-ERα^{Y537C} lines, respectively (Supplementary Fig. S12). Collectively, the CoA recruitment, ERα target gene expression, and proliferation data confirm *in vitro* activity of H3B-5942 across a range of models of endocrine-therapy resistance.

H3B-5942 has potent antitumor activity in ERα^{WT} and ERα^{MUT} breast tumor models

Based on the significant anti-proliferative activity of H3B-5942 in breast cancer cell lines *in vitro*, we next aimed to assess its antitumor activity across various cell line-derived and PDX tumor models harboring ERα^{WT} or ERα^{MUT}. H3B-5942 dosed once (QDx1) orally at 30-300 mg/kg showed a dose-proportional increase in plasma and tumor exposure and a concomitant dose-proportional decrease in expression of ERα target genes, *PGR* and *NPY1R*, in the ERα$^{Y537S/WT}$ ST941 tumor model (Supplementary Fig. S13). Single or repeat dosing of H3B-5942 at 200 mg/kg suppressed a large panel of direct ERα target genes [28] (Supplementary Fig. S14), with QDx1 dosing maintaining target gene suppression for up to 72 hours post-dose, and QDx3 (three daily doses) dosing demonstrating greatest suppression in *PGR* and *NPY1R* (Supplementary Fig. S14).

We first evaluated the efficacy of H3B-5942 administered orally in the MCF7 xenograft model in athymic female nude mice. Once daily oral administration of 1, 3, 10 or 30 mg/kg H3B-5942 resulted in dose-dependent tumor growth inhibition (tumor growth inhibition (TGI) on day 17 of 19%, 41%, 68%, and 83%, respectively) (Supplementary Fig. S15). Whereas the TGI achieved by subcutaneous (SC) tamoxifen treatment at 1 mg/mouse every other day was comparable to that achieved with H3B-5942 (TGI of 80%), once weekly (QW) SC fulvestrant treatment at 5 mg/mouse showed reduced TGI (TGI of 47%). In addition to the ERα^{WT} MCF7 model, H3B-5942 demonstrated significant efficacy across a panel of ERα^{WT} PDX models, inducing stasis or regressions (Supplementary Fig. S16). As expected, no significant TGI was observed in ERα negative PDX models (Supplementary Fig. S16).

Next, we evaluated the antitumor activity of H3B-5942 administered orally QD in the ERα$^{Y537S/WT}$ ST941 model in athymic female nude mice. Oral QD administration of 3, 10, 30,

100 and 200 mg/kg H3B-5942 resulted in dose-dependent inhibition of tumor growth (TGI on day 35 of 3%, 35%, 63%, 76% and 81%, respectively) (Fig. 4C; Supplementary Fig. S17A), and dose-dependent suppression in ERα target genes *PGR* (PR) and *SGK3*, and the proliferation marker Ki67 in endpoint tumors (Fig. 4D; Supplementary Fig. S17B-C). Although tamoxifen and fulvestrant also inhibited tumor growth (TGI of 70% and 30%, respectively), H3B-5942 demonstrated superior activity relative to fulvestrant (Fig. 4C; Supplementary Fig. S17A). Consistent with the significant antitumor activity in the ST941 model, H3B-5942 also demonstrated superior activity over SoCs in an independent $ER\alpha^{Y537S/-}$ endocrine-therapy resistant WHIM20 model (Supplementary Fig. S18). Collectively, *in vivo* profiling confirmed H3B-5942 has significant antitumor activity in both the $ER\alpha^{WT}$ and $ER\alpha^{MUT}$ setting at well-tolerated doses (Supplementary Fig. S19).

H3B-5942 in combination with CDK4/6 or mTOR inhibitors leads to synergistic activity

Although H3B-5942 monotherapy showed potent inhibitory activity in both $ER\alpha^{WT}$ and $ER\alpha^{MUT}$ backgrounds, we next aimed to identify cellular pathways that, upon co-inhibition, might further enhance SERCA potency. To this end, we performed an unbiased *in vitro* combination screen in the PDX-$ER\alpha^{Y537S/WT}$ breast cancer cell line using a fixed concentration of H3B-5942 at 1 μM and multiple doses of a panel of reference compounds including marketed drugs, compounds currently in clinical trials, and tool compounds. The panel consisted of 1356 small molecule inhibitors with 1198 unique structures (11.6% sample redundancy) and 334 unique protein targets. After 6 days exposure to compounds, cell viability/proliferation was determined, and the delta-AUC was calculated for each combination. Data are presented as a waterfall plot (Fig. 5A) showing the combination results as the fold change in standard deviations (STDEV) from the median for the middle 1000 results. The FDA approved CDK4/6

inhibitors palbociclib (n=4), ribociclib (n=2), and abemaciclib (n=2) as well as several mTOR inhibitors clustered as highly synergistic combinations (Fig. 5A, inset and table; Supplementary Fig. S20-21). To confirm the high-throughput combination screening results, traditional matrix-style combination tests were performed. As expected, large areas of synergy were observed with clear effects above 10-25 nM for H3B-5942 and 25 pM and above for the CDK4/6 inhibitors across multiple cell lines bearing $ER\alpha^{WT}$ or clinically frequent ERα mutations (Fig. 5B; Supplementary Fig. S20B). The enhanced anti-proliferative potency observed *in vitro* was supported by greater suppression of proliferation markers *MKI67* and *CDC25A* in the combination setting relative to either monotherapy alone (Supplementary Fig. S22).

To confirm the *in vitro* combination activity with CDK4/6 inhibition, we administered H3B-5942 alone or in combination with palbociclib and monitored efficacy in the MCF7 and ST941 tumor models. Consistent with the *in vitro* analysis, greater efficacy was achieved in the combination setting in both the $ER\alpha^{WT}$ and $ER\alpha^{MUT}$ models (Fig. 5C, D; Supplementary Fig. S23). In aggregate, these data suggest that although H3B-5942 as a monotherapy is very potent, combination therapy with agents that target CDK4/6 or potentially mTOR can further improve potency.

Discussion

Endocrine therapy is a standard treatment option for ER-positive breast cancer patients. Currently, the majority of breast cancer patients with localized disease will experience long-term disease-free survival. Unfortunately, the clinical effectiveness can be limited because of high rates of intrinsic and acquired drug resistance during treatment. Those patients who present with or develop endocrine refractory metastatic diseases have a 5-year survival less than 25% and are

currently incurable [29]. Although it appears that breast cancer develops resistance to endocrine therapies through multiple molecular processes, reactivation of ERα remains a prominent mechanism. The recent discoveries of hotspot ERα mutations in metastatic breast cancer further strengthen the key role of ERα in drug resistance and disease development. The recurrent mutations, mainly occurring on tyrosine-537 and aspartic acid-538 located in the ligand-binding domain, are enriched in nearly 30% of endocrine-therapy resistant metastases and are associated with more aggressive disease biology with shorter overall survival relative to the wild-type ERα [13]. Furthermore, ERα mutations induce ligand-independent activation of the ERα pathway and confer partial resistance to existing classes of endocrine therapies [7-13, 30]. Therefore, there is a critical need to develop the next generation of ERα antagonists that can overcome aberrant activities of both $ER\alpha^{WT}$ and $ER\alpha^{MUT}$.

The existing classes of ER antagonists, SERMs, and SERDs, exploit distinct mechanisms to promote their antitumor activities. SERMs execute selective inhibition or stimulation of estrogen-like actions in a tissue-dependent manner through differential recruitment of coregulators to ERα, which in turn regulates ERα dependent transcription. In contrast, SERDs trigger selective ER degradation upon binding to the ligand binding domain. Hence, SERDs are usually considered as "pure" ER antagonists showing distinct tissue-selective activities compared to SERMs. Given the clinical success of fulvestrant there has been significant efforts geared towards the development of orally bioavailable SERDs or SERD/SERM hybrids. Several oral SERDs have recently been tested in clinical trials for locally advanced or metastatic ER-positive breast cancer, including a nonsteroidal combined SERM and SERD brilanestrant (GDC-0810, discontinued), elacestrant (RAD1901) and AZD9496. Although some are showing encouraging clinical data, none of them were originally developed to target both $ER\alpha^{WT}$ and $ER\alpha^{MUT}$. Thus,

identification of novel classes of ER antagonists that effectively target ERα^{MUT} is of great interest for metastatic breast cancer patients with unmet medical need.

Previously, in order to study the ERα structure and map the ligand binding domain, affinity labeling ligands (estrogenic ketononestrol aziridine and antiestrogenic tamoxifen aziridine) that covalently engaged with ERα were developed [31]. Interestingly, although both preferentially engaged with C530, these ligands were capable of labeling an alternate residue in the absence of C530 [32]. Here, we positioned an internal electrophile so that covalent modification only occurs at C530 located in the ligand-binding domain of ERα.

Similar to SERMs and SERDs, upon binding to ERα, SERCA H3B-5942 triggers global DNA binding of ERα to ERE-containing promoter and enhancer regions, and induces a transcriptionally repressive conformation of ERα by evicting coactivators. H3B-5942 also shares some pharmacological features with SERMs, e.g., the uterotrophic activity observed in immature rats. Importantly, H3B-5942 demonstrates a distinct MoA from other ERα antagonists. H3B-5942 induces a unique conformational change of ERα that is distinct from SERDs and SERMs as revealed by a peptide mapping reporter system. Subsequently, H3B-5942-bound ERα differentially regulates a subset of target genes in endometrial carcinoma cells, suggesting it may possess less ERα agonistic activity compared with SERMs in certain cellular contexts. The covalency of H3B-5942 appears to contribute at least some of these unique profiles since the chemical analog of H3B-5942 lacking the Michael acceptor (H3B-9224) or genetic disruption of the covalency (C530S mutation in ERα) largely abolished the gain in anti-ERα potency by the unique MoA. However, it is currently unclear whether enhanced residence time on ER and/or potentially different conformational states that may exist following H3B-5942/-9224 binding is contributing to the differential functional profiles.

Since H3B-5942 shows a clear dependence on covalent engagement, it is conceivable that resistant mechanisms may occur by mutation of C530 in ERα. Therefore, development of next generation SERCAs with alternate interactions between the core of the molecule and the ligand binding domain may influence binding affinity, residence time and/or conformational state of the protein, all of which may potentially help to overcome C530-related resistance and maintain downstream potency associated with covalent engagement.

In summary, we identified a class of selective estrogen receptor covalent antagonist that demonstrates preclinical evidence of covalent binding to ERα, potent inhibition of ERα-dependent transcription, and antitumor activity in both $ER\alpha^{WT}$ and $ER\alpha^{MUT}$ breast tumor models.

Methods

Cell Lines

MCF7 BUS cells [33] were maintained in Dulbecco's Modified Eagle Medium (DMEM) supplemented with 10% FBS, 4 mM L-glutamine and 1x non-essential amino acids. MCF7 lines engineered to overexpress $ER\alpha^{WT}$, $ER\alpha^{Y537S}$, $ER\alpha^{Y537C}$, $ER\alpha^{Y537N}$, $ER\alpha^{D380Q}$, $ER\alpha^{WT/C530S}$ and $ER\alpha^{Y537S/C530S}$ were derived from the MCF7 BUS cells and similarly maintained in culture. MCF7(P)-AP2, a serially *in vivo* passaged cell line derived from the MCF7-ATCC tumors, was cultured in EMEM media supplemented with 10% FBS and used for xenograft studies. MCF7-Parental cell lines derived from ATCC were cultured in phenol red-free RPMI supplemented with 10% FBS and exogenous estradiol (1nM). The respective LTED derivatives, MCF7-LTED-$ER\alpha^{WT}$ and MCF7-LTED-$ER\alpha^{Y537C}$ were cultured, as previously described [34] in phenol red-free RPMI supplemented with 10% dextran charcoal-stripped FBS (DCC medium). MDA-MB-231 cells were maintained in Leibovitz's L-15 media supplemented with 10% FBS. The PDX-$ER\alpha^{Y537S/WT}$ cell line was derived from a patient-derived xenograft tumor model and was routinely cultured in DMEM supplemented with 20% FBS. Lenti-X 293T cells (Clontech, cat # 632180) were routinely cultured in DMEM supplemented with 10% FBS and 4 mM L-glutamine. Ishikawa cells were maintained in MEM supplemented with 2 mM L-glutamine, 1% non-essential amino acids and 5% FBS. All cells were maintained prior to and during experiments at 37º C, 5% CO_2, and at 95% relative humidity. Cells were passaged 2 to 3 times per week and passage number was limited to between 6 and 20. For *in vitro* experiments, cells were seeded at appropriate densities to provide logarithmic growth during, and at least 24 hours beyond, the experiment duration. All cell lines were verified to be free of Mycobacterium contamination, and their identity was confirmed by short tandem repeat analysis of 9 markers.

Protein production and purification

E.coli codon-optimized genes encoding the ligand-binding domains of the receptors His-TEV-ERα-WT (297-554), His-TEV-ERα-Y537S (297-554), His-TEV-ERα-C530S (297-554), His-TEV-ERα-C530S-Y537S (297-554), His-TEV-ERα-C381S-C417S (307-554) and His-TEV-ERα-C381S-C417S-Y537S (307-554) were synthesized by Genewiz and cloned into pET28a (EMD Millipore). Proteins were expressed in Escherichia coli overnight at 12-16 °C after induction with 0.5 mM IPTG at an OD600 of ~0.8. Soluble protein was purified by Ni-NTA chromatography followed by size exclusion chromatography on a 26/60 Superdex S-200 column equilibrated in 50 mM Tris-HCl, pH 8.0, 150 mM NaCl, 5-10% glycerol, and 1 mM TCEP. For mass spectrometry and crystallography applications, the His-tag was removed after the Ni-NTA step with overnight TEV protease incubation. The cleaved proteins were then injected on the gel filtration column as described above. Peak fractions were pooled and flash frozen in liquid nitrogen.

Crystallography

His-TEV-ERα^{Y537S} (307-554) was cloned into pET-28a (EMD Millipore) and expressed in E coli. In this construct, two surface exposed cysteine mutations, C381S and C417S, were introduced to improve protein behavior and yields. Soluble protein was obtained by overnight induction at 20° C using 0.1 mM IPTG [35]. Cells were harvested and protein was purified using Ni-NTA chromatography followed by overnight TEV cleavage of the His-tag and a polishing subtractive Ni-NTA step to remove the TEV. The flow-through was concentrated and injected on a sephacryl S-300 column equilibrated in 50 mM Tris pH 8, 150 mM NaCl, 1 mM TCEP, and

10% glycerol. Peak fractions were pooled and concentrated to ~12.4 mg/ml and flash frozen in liquid nitrogen. Co-crystals were obtained by mixing compound and protein at 2:1 molar ratio at room temperature for 1 hour to allow time for covalent bond to form, followed by filtration to remove aggregates. Sitting drops were set up using 0.5 µL protein + 0.5 µL reservoir and equilibrated over a reservoir containing 4-12% PEG 3350, 50-200 mM $MgCl_2$, and 100 mM imidazole pH 7.1. Crystals grew to full size in 1-3 weeks and flash frozen using reservoir solution supplemented with 20% ethylene glycol. Data were collected by Shamrock Structures LLC at the Advanced Photon Source, LS-CAT 21-ID-G. The structure was solved by molecular replacement using MOLREP [36] and refined using Refmac [37] with ligand coordinates generated using JLigand. The PDB identification code for H3B-5942 is 6CHW, and for H3B-9224 is 6CHZ.

Intact mass spectrometry to assess covalency of H3B-5942

ERα-WT (297-554) and mutant proteins (297-554) were incubated in 50 mM Tris pH 8.0, 150 mM NaCl, 5% glycerol and 1 mM TCEP with a 2-fold excess of compound (2 µM H3B-5942: 1 µM ERα protein solution) at 4^0C overnight. Mass analyses were carried out on a Thermo Scientific Q-Exactive HRM (ESI source, 4.0kV ionization voltage, 250^0C capillary temp., 10 arb sheath gas, S-lens RF level 65) coupled with an Accela Open AS 1250. Samples (10 µL) were desalted on a C4 column (Thermo Scientific Accucore 2.1x150 mm, 2.6 µm) with a gradient from 5% to 95% B over 10 minutes. Eluent A consisted of 0.1% formic acid in water, and eluent B consisted of 0.1% formic acid in acetonitrile. The flow was set to 400 nL/min. All solvents were LC/MS grade (Thermo Scientific). The mass spectrometer was run in positive

mode collecting full scan at R=70,000 from *m/z* 500 to *m/z* 2000. Data was collected with the Xcalibur 3.1 software.

Xcalibur raw files were processed using BioPharma Finder 2.0 (Thermo Scientific) and the ReSpect deconvolution algorithm. Peak was averaged over selected retention time to generate source spectra from TIC chromatogram trace, and the chromatogram parameters set to *m/z* 700 to 2000. Outputs for deconvolution algorithm include model mass range from 10,000 to 160,000, mass tolerance 20 ppm, charge state range from 10 to 100, target mass is the estimated mass of protein or protein + compounds, with noise rejection of 95% confidence.

Estradiol K_d Measurements

Varying amounts of ^{3}H-estradiol (Perkin Elmer, cat. # NET517250UC) were diluted into 1480 µL of binding buffer (25 mM Tris pH 8.0, 10% Glycerol, 1 mM TCEP, 0.3 mg/mL ovalbumin) in a 2 mL microfuge tube (VWR, cat. #10025-738). His-TEV-ERα-C381S-C417S (307-554) or His-TEV-ERα-C381S-C417S-Y537S (307-554) was then added to the ^{3}H-estradiol solution at a final concentration of 25 pM (WT) or 5 pM (Y537S). The final volume of the mixture was 1500 µL. Binding was allowed to equilibrate at 4 ºC for 18 hours. Following the 18 hour incubation, 300 µL of hydroxyapatite (HAP) resin (Bio-Rad, cat. # 1300150) was added to the binding mixture, and the 2 mL tube was rotated at room temperature for 1 hour. The HAP resin with ^{3}H-estradiol- ERα complex bound was then washed in the 2 mL microfuge tube three times with 900 µL of 25 mM Tris pH 7.2. For the ERα-WT-estradiol binding measurements, the HAP resin was resuspended in 200 µL of dH_20 and transferred to a scintillation vial containing 3 mL of MicroScint-PS scintillation fluid (Perkin-Elmer, cat. # 6013631) prior to reading with a

MicroBeta2 scintillation counter. Due to the very low amounts of ERα-Y537S used in each 2 mL tube, the HAP resin from two 2 mL binding reactions was combined into one scintillation vial prior to reading so as to achieve a suitable signal to noise ratio.

K_d values were determined in Prism using the following equation:

$Y = Y_{max}/(1 + K_d/ [L])$

Ligand K_i Measurements

100 pM His-TEV-ERα-C381S-C417S (307-554) or His-TEV-ERα-C381S-C417S-Y537S (307-554), 1 nM ^{3}H-estradiol and varying concentrations of competitor ligand were mixed in binding buffer (25 mM Tris pH 8.0, 10% Glycerol, 1 mM TCEP, 0.3 mg/mL ovalbumin) at a final volume of 1200 µL. ERα-ligand binding was allowed to equilibrate for 18 hours at 4 ºC. 300 µL of HAP was then added to the binding mixture and the 2 mL tube rotated at room temperature for 1 hour. The HAP resin with the ^{3}H-estradiol- ERα complex bound was then washed in the 2 mL microfuge tube three times with 900 µL of 25 mM Tris pH 7.2. The HAP resin was then resuspended in 200 µL of dH_20 and transferred into a scintillation vial containing 3 mL of scintillation fluid and read on a scintillation counter as described above. K_i values were calculated using the Munson and Rodbard equation [38].

Jump Dilution Experiment

His-TEV-ERα-C381S-C417S (307-554) or His-TEV-ERα-C381S-C417S-Y537S (307-554) and ligand were diluted into 75 µL of binding buffer (25 mM Tris pH 8.0, 10% Glycerol, 1 mM TCEP, 0.3 mg/mL ovalbumin) at a concentration of 4 nM ERα protein and 10 nM ligand, in

a 2 mL microfuge tube. The ERα-ligand mixture was allowed to sit at room temperature for 5 hours to achieve binding equilibrium.

After 5 hours, the binding mixture was diluted to a final volume of 1500 µL with binding buffer in the presence of 7.5 nM ^{3}H-estradiol. The final concentrations of ERα and ligand were 200 pM and 500 pM, respectively. Under these final diluted conditions, the concentration of ^{3}H-estradiol is 15-fold greater than competitor ligand. The diluted binding mixture was placed at 4 ºC for 22 hours, during which time the free ^{3}H-estradiol replaces the pre-bound ligand after it dissociates from ERα. After the 22 hour incubation at 4 ºC, the ERα-^{3}H-estradiol complex was bound to HAP resin, washed and read on a scintillation counter as described above.

ERα^{WT} and ERβ^{WT} binding assays

Both Enzyme Fragment Complementation (EFC)-based assays were performed at DiscoverX using components of the HitHunter Estrogen Assay Kit (cat # 90-0019). Purified recombinant full length human ERα and ERβ proteins were obtained from Life Technologies (ERα: cat # A15674; ERβ: cat # A15664). During assay optimization, the concentration of ERα or ERβ protein was titrated into the assay based on the molecular weight of each protein (ERα: 53.4 kDa and ERβ: 66.4 kDa) to produce a comparable EC_{50} with the reference ligand, 17β-estradiol. All test compounds were serially diluted (1:3) in DMSO, prepared at 46X the final assay concentration. In brief, 2 µL of compound titration (10 µmol/L starting dose; 11-point dose response, plus DMSO only control; 4 replicates/dose), 20 µL ED reagent, and 30 µL of a 2.5 µg/mL stock of ERα or 1.6 µg/mL of ERβ protein were added to each well of a 96-well assay plate. The assay components were incubated for 90 minutes at room temperature. Following

incubation, HitHunter Detection reagent was prepared as recommended by the manufacturer (DiscoverX) and then added to each plate, followed by a 1 hour incubation at room temperature in the dark. The assay plate was read on an Envision plate reader (Perkin Elmer) and data were analyzed using the GraphPad Prism software. Data from each sample (average of quadruplicate wells) was normalized to the max value for the reference sample, 17β-estradiol, to calculate percentage activity. The EC_{50} was calculated using the equation: log(agonist) vs. response—variable slope (4 parameters). Three independent assays were conducted on separate days.

Co-regulator Peptide Recruitment to ERα (TR-FRET)

Assay buffer was comprised of 100 mM potassium phosphate, pH 7.4, 5 mM DTT, 0.1 mg/mL bovine gamma-globulin, and 0.001% pluronic F-127. A 2x working stock of His-ERα-LBD was prepared by diluting the protein to 4 nM in assay buffer. Solutions of 5x anti-6xHis-Terbium antibody (CisBio, 61HISTLA) and 3.33x fluorescently labeled peptide (Thermo Fisher) were prepared separately such that their final concentrations were 3 and 125 nM. Fluorescently labeled biotin was also included to control for non-specific binding.

An acoustic dispenser delivered 2 nL compound or DMSO for a final concentration of 2 µM in 384-well assay plates (Corning, 3820). Then, 5 µL of 2x protein working stock or controls were added. Plates were centrifuged, and incubated for 1 hour at room temperature, followed by addition of 3 µL of fluorescently labeled peptide and 2 µL of 5x antibody. Plates were covered, centrifuged, and incubated for an additional hour. The positive control contained His-ERα-LBD protein, PGC1α peptide, and 50 nM (final) estradiol or DMSO for the wild-type or mutant protein, respectively. The negative controls were the same but lacked ERα.

The TR-FRET data was recorded with an Envision plate reader (Perkin Elmer), using the settings recommended by Thermo Fisher. Normalization of TR-FRET signal to percent

activation and Z' values were determined from the positive and negative control's recruitment of FITC-PGC1α. Experiments were performed in triplicate and data were analyzed in GraphPad Prism 7.

Co-regulator Peptide Recruitment to ERα (MARCoNI)

ERα from the lysate of serum-starved MCF7 was functionally analyzed by MARCoNI as described previously [39]. Each array was incubated with ERα containing lysate in the presence of compound or solvent (DMSO) only. The negative control (DMSO) and positive control (17β-estradiol were analyzed using 4 technical replicates (arrays) each. 4-OHT and H3B-5942 test compounds were analyzed using 3 technical replicates. Binding was detected with fluorescently labeled ERα antibody. From each array, a series (increasing exposure time) of tiff images were obtained by the CCD camera in the PamStation (incubator). The signal intensity (arbitrary units fluorescence) of each interaction/array/exposure time/array was quantified using dedicated BioNavigator software (PamGene). A circle was placed around the spot boundaries, and the signal within (foreground) and just outside (background) was determined. For each interaction, the exposure time series signal minus background values were used for a linear fit, from which the signal at 100 ms was extracted. Next, we applied a cut-off at the bottom of the signal range to eliminate noise: all signals < 50 are set to 50.

Cellular PGC1α recruitment to ERα^{WT} in CHO-K1 cells

The cellular EFC-based CoA recruitment assay was performed at DiscoverX using conditions previously established. In brief, CHO-K1 cells expressing full-length human ERα fused to an enzyme donor and full-length PGC1α containing steroid receptor co-activator

peptide (SRCP) domains fused to an enzyme acceptor were counted and resuspended in PathHunter Cell Plating Reagent 13 (cat # 93-0563R13A) containing charcoal-dextran stripped FBS and seeded into 384-well assay plates at 10,000 cells per well in 20 µL. Compounds were serially diluted (1:3) in PBS+1% BSA in 12-point dose response format, 4 replicates per concentration. The last well in the dilution series was DMSO only. Intermediate dilutions of ERα antagonists from the original stock was performed in DMSO, followed by a 1:20 dilution in PBS + 0.1% BSA to generate a 5X stock. 5 µL of compound dilution was added to the appropriate wells and incubated for 1 hour at 37º C. Cells were then stimulated by exposure to 17β-estradiol (20 nM final concentration; 5 µL of a 6X stock) for 6 hours at 37º C. PathHunter chemiluminescent detection reagents were prepared as recommended by the manufacturer; 15 µL of reagent was added per well, and the plates incubated at room temperature for 1 hour in the dark. Luminescence signal was captured for each well on an Envision plate reader (Perkin Elmer). Signals were normalized to basal activity of the 17 β -estradiol agonist control curve on each plate. Three independent assays were conducted on separate days.

Cellular CoA recruitment analysis to AR, MR, GR and PRα/β

The selectivity assay principle is similar to that of the ERα CoA recruitment assay described above. However, the control agonists and antagonists varied for each NHR tested. The control agonists used were: 6α-Fluorotestosterone for Androgen Receptor (AR), Aldosterone for Mineralocorticoid Receptor (MR), Dexamethasone for Glucocorticoid Receptor (GR) and Norgestrel for Progesterone Receptor alpha/beta (PRα/β). The control antagonists used were: Mifepristone for GR and Geldanamycin for AR, MR, and PRα/β. In brief, cells were seeded in a total volume of 20 µL into white 384-well microplates and incubated at 37º C prior to testing.

Assay media contained charcoal-dextran filtered serum to reduce hormone levels. Intermediate dilution of test agent stocks was performed to generate 5x test agent in assay buffer. 5 μL of 5x compound was added to cells and incubated at 37º C for 1 hour. Vehicle concentration was 1%. 5 μL of 6x EC_{80} agonist (EC_{80} concentrations were: 0.03 μM 6α-Fluorotestosterone, 0.005 μM Aldosterone, 0.12 μM Dexamethasone, 0.005 μM Norgestrel) in assay buffer was added to the cells and incubated at 37º C for 6 hours. Assay signal was generated through the addition of 15 μL (50% v/v) of PathHunter Detection reagent cocktail, followed by 1-hour incubation at room temperature. Microplates were read following signal generation with an Envision plate reader (Perkin Elmer) for chemiluminescent signal detection.

Cellular recruitment of LXXLL peptides and conformationally sensitive peptides

Estradiol (E2), 4-hydroxytamoxifen (4-OHT), tamoxifen, and fulvestrant were purchased from Sigma. For the estrogen receptor conformation profiling assay, a panel of validated cofactors was tested for their ability to interact with ER when bound by mechanistically distinct ER antagonists. In addition to the receptor interacting domains (IDs), isolated NR boxes (e.g., ACTR NR box 1 and 2) from the aforementioned cofactors were tested in isolation from the IDs. Various recombinant LXXLL (coactivator-receptor binding motif) and corepressor nuclear receptor (CoRNR) box peptides were also tested in this manner. HepG2 cells were maintained in Basal Medium Eagles containing 8% fetal bovine serum. For mammalian two-hybrid based ER cofactor assay, cells were seeded in 96-well plates and transfected with VP16-ER (900 ng), 5XGalLuc3 (900 ng), Gal4-interactor (900 ng), and Renilla-Luc (300 ng) using Lipofectin. Cells were then treated with saturating concentrations of ligand (10 μM for ER antagonist) for 48 hours, at which point, dual luciferase assays were performed. The data were standardized to

avoid bias due to signal strength and clustered with the Ward hierarchical clustering method using JMP (SAS). The hierarchical cluster dendrogram was ordered by the first principal component. Data were clustered using the UPGMA (**U**nweighted **P**air **G**roup **M**ethod with **A**rithmetic Mean) method, and correlation distance was measured using Spotfire (spotfire.tibco.com).

Immunoblot analysis in whole cell lysates

Cells were lysed in loading buffer (Invitrogen, cat # NP0007) containing protease inhibitor (Roche, cat # 05892791001) and DTT (Invitrogen, cat # NP0009), sonicated and subsequently boiled for 5 minutes. Approximately 30 μg of protein was loaded per lane and resolved by SDS polyacrylamide electrophoresis. Protein was transferred onto nitrocellulose membranes, blocked in 5% low-fat milk and probed overnight with antibodies to Estrogen Receptor (ER) (SP1) (Spring Bioscience, cat # M3012), Rb (4H1) (Cell Signaling, cat # 9309), Phospho-Rb (Ser780) (D59B7) (Cell signaling, cat # 8180), Cyclin D1 [EPR2241] (Abcam, cat # ab134175), α-Tubulin (Sigma, cat # T6199), and GAPDH (Sigma, cat # G9545). Membranes were incubated with horseradish peroxidase (HRP)-conjugated anti-rabbit secondary antibody (Cell Signaling, cat # 7074) or anti-mouse secondary antibody (Cell Signaling, cat # 7076) for 1 hour and signal was developed using the ECL method (GE Healthcare).

MCF7 Xenograft Generation, Dosing, and Measurement of Antitumor Activity

When preparing the MCF7(P)-AP2 cells for *in vivo* studies, the cells were harvested and washed with PBS, incubated with 0.25% trypsin-EDTA, and suspended in a 1:1 mixture of Matrigel (Corning 354234) and Hank's Balanced Salt Solution (HBSS) at a final concentration of 5 $x10^7$ cells/ mL. To generate xenografts, 0.2 mL of the inoculum was injected into the 3rd

mammary fat pad of 6-8 week old female Balb/c nude mice (Balb/cOlaHsd-*Foxn1*^{nu}), giving a final concentration of 1 x 10^7 cells/ mouse. Three days prior to inoculation, each mouse was implanted with a 0.72 mg 90-day release estrogen pellet (Innovative Research of America). When the mean tumor volume (TV) reached approximately 150-200 mm^3, animals were selected based on TV and randomized into treatment groups of 6-8 animals per group. Single agent or combination treatments were started on Day 0 and continued for the duration of the study. H3B-5942 was administered PO QD, tamoxifen was given SC Q2D, fulvestrant was given SC QW, and palbociclib was administered PO QD. Each treatment was administered based on body weight (10 mL/kg). H3B-5942 was formulated daily in 10% 2-Hydroxypropyl-β-CycloDextrin (HPβCD) in 5% dextrose, tamoxifen was formulated in 95% peanut oil/5% ethanol (EtOH), clinical grade fulvestrant was administered, and palbociclib was formulated in 25 mM sodium bicarbonate, 15 mM lactic acid solution with 2% Cremaphor EL. The body weight (BW) measurements were performed daily, and tumor measurements were recorded twice a week.

The TV in mm^3 was calculated according to the following formula:

$TV = length \times width^2 \times 0.5$
length: largest diameter of tumor (mm)
width: diameter perpendicular to length (mm)

The Tumor Growth Inhibition% (TGI) was calculated according to the following formula:

Tumor Growth Inhibition% (TGI) =

$$\frac{\text{Average Control TV Day X} - \text{Treatment TV Day X}}{\text{Average Control TV Day X}} \times 100$$

where Day X is any day of measurement.

All procedures relating to animal care, handling, and treatment were performed according to guidelines approved by the Institutional Animal Ethics Committee (IAEC) of Aurigene

Discovery Technologies Ltd. All doses and regimens were well tolerated with no clinical signs observed in all studies presented.

ERα$^{Y537S/WT}$ ST941 PDX tumor Xenograft Generation, Dosing, and Measurement of Antitumor Activity

The ST941 PDX model representing an ERα$^{Y537S/WT}$ mutated human ER+ breast cancer was propagated in mice. To generate patient-derived xenografts, solid tumor tissues from the ERα$^{Y537S/WT}$ positive xenograft model (passage 6) were cut into 70 mg pieces, mixed with Matrigel (Corning, 354234) and subcutaneously implanted into the right flank of 12 week old female athymic Nude (Crl:NU(NCr)-Foxn1nu) mice supplied with drinking water containing estradiol (Sigma-Aldrich, cat # E1024-25G). When the mean TV reached approximately 125-200 mm^3, animals were selected based on TV and randomized into treatment groups of 6-8 animals per group. H3B-5942 was administered PO QD (same formulation as above), tamoxifen was given SC TIW, fulvestrant was given SC QW, and palbociclib was dosed PO QD. Each treatment was administered based on body weight (10 mL/kg), except tamoxifen and fulvestrant which were flat-dosed. Tamoxifen was formulated in 90% peanut oil/10% EtOH, and clinical grade fulvestrant was administered without further dilution. Beginning three days prior to treatment and for the remainder of the study, exogenous estradiol was removed from the drinking water. BW measurements were performed daily and TV measurements were recorded twice per week. All studies were performed under guidelines set forth by the South Texas Accelerated Research Therapeutics (START) IACUC and defined in the START Animal Care and Use Program (Protocol 09-001). All doses and regimens were well tolerated.

End-of-study tumor samples were formalin-fixed and paraffin-embedded (FFPE) at START and subsequently shipped to Cancer Genetics Inc. for sectioning, staining, and RNA

extraction. In brief, five-micrometer sections of FFPE tissue xenograft samples were stained for ERα, Progesterone Receptor (PR) and Ki67 using the Ventana rabbit monoclonal primary antibodies ER (SP1), PR (1E2) and Ki-67 (30-9). IHC assays were run on the Ventana BenchMark IHC/ISH automated slide staining instrument with *ultra*View Universal DAB detection kit. ER, PR and Ki-67 stained slides were scored for % positive tumor cells by a board certified MD-pathologist at Cancer Genetics Inc. Scanned images, pathologist scores, and interpretations were made available to H3 Biomedicine Inc., for review and data analysis.

For gene expression analysis, a custom Nanostring nCounter code set was used with 300 ng of purified total RNA extracted from 60 μm of FFPE blocks using the Qiagen RNAeasy FFPE kit according to the manufacturer's instructions. The RNA was hybridized with the codeset and processed according to the Nanostring's instructions. The nCounter Digital Analyzer counted and tabulated the signals of reporter probes, and the raw counts were normalized to housekeeper.

ERα^{Y537S} WHIM20 PDX tumor Xenograft Generation, Dosing, and Measurement of Antitumor Activity

The WHIM20 PDX model representing an ERα^{Y537S} mutated human ER+ breast cancer was propagated in mice. For the current study, solid tumor tissues were depleted of necrotic components, cut into fragments, mixed with Matrigel and subcutaneously implanted into the right flank of 6-8 week old female SCID-bg mice. The precise number of fragments and volume of matrigel was determined on a case by case basis. When the average TV reached approximately 350-400 mm^3, animals were selected based on TV and randomized into treatment groups of 7-9 animals per group. H3B-5942 was administered PO QD, tamoxifen (formulated in

95% peanut oil/5% EtOH) was administered SC Q2D, and clinical grade fulvestrant was administered SC QW. Each treatment was administered based on body weight (10mL/ kg). BW measurements were performed daily, and TV measurements were recorded twice per week. Mice with at least 20% body weight loss compared with Day 0 body weight were euthanized to prevent any pain or suffering to the animal. All procedures relating to animal care, handling and treatment were performed according to guidelines approved by the Institutional Animal Ethics Committee (IAEC) of Aurigene Discovery Technologies Ltd.

Statistical analysis

In vitro data are expressed as mean ± SEM or mean ± SD as indicated. Statistical significance was determined by two-sided t-test analysis. Uterotrophic data are presented as mean ± SD and were analyzed using a two-sided t-test. Efficacy data are expressed as mean ± SEM for TV. The differences in TV on the final day of TV measurements between the vehicle and treatment groups were analyzed by multiple unpaired t-tests with significance determined using the Holm-Sidak method with alpha set to 0.05 and without assuming a consistent standard deviation. Statistical analyses were performed using GraphPad Prism version 5.04 (GraphPad Software, La Jolla, CA).

Accession Number

Microarray, RNA-seq and ChIP-seq data presented in the manuscript has been deposited at the National Center for Biotechnology Information (NCBI) Gene Expression Omnibus with the accession number GSE115611.

Additional experimental procedures are listed in the Supplementary Methods.

Acknowledgments

We would like to thank Raghuveer Ramachandra for assistance with the MCF7 tumor model development and subsequent efficacy studies. We would also like to thank Drs. Tarek Sahmoud and Rinath Jeselsohn for helpful discussions. This work was supported by H3 Biomedicine, Inc. Additional funding was generously provided by the Breast Cancer Now Toby Robins Research Centre, and NHS funding to The Royal Marsden Hospital's NIHR Biomedical Research Centre (L.A.M., S.P., R.R.).

References

1. Kauhava, L., et al., *Lower recurrence risk through mammographic screening reduces breast cancer treatment costs.* Breast, 2008. **17**(6): p. 550-4.
2. Spicer, D.V. and M.C. Pike, *Breast cancer prevention through modulation of endogenous hormones.* Breast cancer research and treatment, 1993. **28**(2): p. 179-93.
3. Beslija, S., et al., *Third consensus on medical treatment of metastatic breast cancer.* Annals of oncology : official journal of the European Society for Medical Oncology, 2009. **20**(11): p. 1771-85.
4. Shou, J., et al., *Mechanisms of tamoxifen resistance: increased estrogen receptor-HER2/neu cross-talk in ER/HER2-positive breast cancer.* Journal of the National Cancer Institute, 2004. **96**(12): p. 926-35.
5. Musgrove, E.A. and R.L. Sutherland, *Biological determinants of endocrine resistance in breast cancer.* Nature reviews. Cancer, 2009. **9**(9): p. 631-43.
6. Osborne, C.K., et al., *Role of the estrogen receptor coactivator AIB1 (SRC-3) and HER-2/neu in tamoxifen resistance in breast cancer.* Journal of the National Cancer Institute, 2003. **95**(5): p. 353-61.
7. Li, S., et al., *Endocrine-therapy-resistant ESR1 variants revealed by genomic characterization of breast-cancer-derived xenografts.* Cell reports, 2013. **4**(6): p. 1116-30.
8. Robinson, D.R., et al., *Activating ESR1 mutations in hormone-resistant metastatic breast cancer.* Nature genetics, 2013. **45**(12): p. 1446-51.
9. Toy, W., et al., *ESR1 ligand-binding domain mutations in hormone-resistant breast cancer.* Nature genetics, 2013. **45**(12): p. 1439-45.
10. Merenbakh-Lamin, K., et al., *D538G mutation in estrogen receptor-alpha: A novel mechanism for acquired endocrine resistance in breast cancer.* Cancer research, 2013. **73**(23): p. 6856-64.
11. Yu, M., et al., *Cancer therapy. Ex vivo culture of circulating breast tumor cells for individualized testing of drug susceptibility.* Science, 2014. **345**(6193): p. 216-20.
12. Segal, C.V. and M. Dowsett, *Estrogen receptor mutations in breast cancer--new focus on an old target.* Clinical cancer research : an official journal of the American Association for Cancer Research, 2014. **20**(7): p. 1724-6.
13. Chandarlapaty, S., et al., *Prevalence of ESR1 Mutations in Cell-Free DNA and Outcomes in Metastatic Breast Cancer: A Secondary Analysis of the BOLERO-2 Clinical Trial.* JAMA oncology, 2016. **2**(10): p. 1310-1315.
14. Fanning, S.W., et al., *Estrogen receptor alpha somatic mutations Y537S and D538G confer breast cancer endocrine resistance by stabilizing the activating function-2 binding conformation.* eLife, 2016. **5**.
15. Nettles, K.W., et al., *NFkappaB selectivity of estrogen receptor ligands revealed by comparative crystallographic analyses.* Nature chemical biology, 2008. **4**(4): p. 241-7.
16. Joseph, J.D., et al., *The selective estrogen receptor downregulator GDC-0810 is efficacious in diverse models of ER+ breast cancer.* eLife, 2016. **5**.
17. Wardell, S.E., et al., *Bazedoxifene exhibits antiestrogenic activity in animal models of tamoxifen-resistant breast cancer: implications for treatment of advanced disease.* Clinical cancer research : an official journal of the American Association for Cancer Research, 2013. **19**(9): p. 2420-31.
18. Iannone, M.A., et al., *Correlation between in vitro peptide binding profiles and cellular activities for estrogen receptor-modulating compounds.* Molecular endocrinology, 2004. **18**(5): p. 1064-81.
19. Norris, J.D., et al., *Peptide antagonists of the human estrogen receptor.* Science, 1999. **285**(5428): p. 744-6.

20. Paige, L.A., et al., *Estrogen receptor (ER) modulators each induce distinct conformational changes in ER alpha and ER beta.* Proceedings of the National Academy of Sciences of the United States of America, 1999. **96**(7): p. 3999-4004.
21. Anzai, Y., et al., *Stimulatory effects of 4-hydroxytamoxifen on proliferation of human endometrial adenocarcinoma cells (Ishikawa line).* Cancer research, 1989. **49**(9): p. 2362-5.
22. Hegy, G.B., et al., *Carboxymethylation of the human estrogen receptor ligand-binding domain-estradiol complex: HPLC/ESMS peptide mapping shows that cysteine 447 does not react with iodoacetic acid.* Steroids, 1996. **61**(6): p. 367-73.
23. Gangloff, M., et al., *Crystal structure of a mutant hERalpha ligand-binding domain reveals key structural features for the mechanism of partial agonism.* The Journal of biological chemistry, 2001. **276**(18): p. 15059-65.
24. Hartman, S.J., *et al*., *The pharmacological effects of estrogen receptor alpha Y537S and D538G mutations.* AACR 2017, 2017. **Abstract 3621**.
25. Carlson, K.E., et al., *Altered ligand binding properties and enhanced stability of a constitutively active estrogen receptor: evidence that an open pocket conformation is required for ligand interaction.* Biochemistry, 1997. **36**(48): p. 14897-905.
26. Koppen, A., et al., *Nuclear receptor-coregulator interaction profiling identifies TRIP3 as a novel peroxisome proliferator-activated receptor gamma cofactor.* Molecular & cellular proteomics : MCP, 2009. **8**(10): p. 2212-26.
27. Martin, L.A., et al., *Discovery of naturally occurring ESR1 mutations in breast cancer cell lines modelling endocrine resistance.* Nature communications, 2017. **8**(1): p. 1865.
28. Bourdeau, V., et al., *Mechanisms of primary and secondary estrogen target gene regulation in breast cancer cells.* Nucleic acids research, 2008. **36**(1): p. 76-93.
29. Rugo, H.S., et al., *Endocrine Therapy for Hormone Receptor-Positive Metastatic Breast Cancer: American Society of Clinical Oncology Guideline.* Journal of clinical oncology : official journal of the American Society of Clinical Oncology, 2016. **34**(25): p. 3069-103.
30. Jeselsohn, R., et al., *Emergence of constitutively active estrogen receptor-alpha mutations in pretreated advanced estrogen receptor-positive breast cancer.* Clinical cancer research : an official journal of the American Association for Cancer Research, 2014. **20**(7): p. 1757-1767.
31. Harlow, K.W., et al., *Identification of cysteine 530 as the covalent attachment site of an affinity-labeling estrogen (ketononestrol aziridine) and antiestrogen (tamoxifen aziridine) in the human estrogen receptor.* The Journal of biological chemistry, 1989. **264**(29): p. 17476-85.
32. Reese, J.C. and B.S. Katzenellenbogen, *Mutagenesis of cysteines in the hormone binding domain of the human estrogen receptor. Alterations in binding and transcriptional activation by covalently and reversibly attaching ligands.* The Journal of biological chemistry, 1991. **266**(17): p. 10880-7.
33. Coser, K.R., et al., *Global analysis of ligand sensitivity of estrogen inducible and suppressible genes in MCF7/BUS breast cancer cells by DNA microarray.* Proceedings of the National Academy of Sciences of the United States of America, 2003. **100**(24): p. 13994-9.
34. Ribas, R., et al., *Identification of chemokine receptors as potential modulators of endocrine resistance in oestrogen receptor-positive breast cancers.* Breast cancer research : BCR, 2014. **16**(5): p. 447.
35. Norman, R.A., et al., *Protein-ligand crystal structures can guide the design of selective inhibitors of the FGFR tyrosine kinase.* Journal of medicinal chemistry, 2012. **55**(11): p. 5003-12.
36. Vagin, A. and A. Teplyakov, *Molecular replacement with MOLREP.* Acta crystallographica. Section D, Biological crystallography, 2010. **66**(Pt 1): p. 22-5.

37. Murshudov, G.N., A.A. Vagin, and E.J. Dodson, *Refinement of macromolecular structures by the maximum-likelihood method.* Acta crystallographica. Section D, Biological crystallography, 1997. **53**(Pt 3): p. 240-55.
38. Munson, P.J. and D. Rodbard, *An exact correction to the "Cheng-Prusoff" correction.* Journal of receptor research, 1988. **8**(1-4): p. 533-46.
39. Jeselsohn, R., et al., *Allele-Specific Chromatin Recruitment and Therapeutic Vulnerabilities of ESR1 Activating Mutations.* Cancer cell, 2018. **33**(2): p. 173-186 e5.

Figure Legends

Figure 1.

Identification of H3B-5942, first-in-class Selective Estrogen Receptor Covalent Antagonist (SERCA). **A,** ERα positive MCF7 breast cancer cell line was engineered to overexpress wild-type and hotspot variants of ERα. Parent, MCF7 parental line; Vector, MCF7 vector control line; $ERα^{WT}$, $ERα^{WT}$ overexpressing MCF7 line; $ERα^{Y537S/N/C/D538G/E380Q}$, designated hotspot ERα mutant overexpressing MCF7 lines. α-tubulin served as loading control. **B,** Heatmap showing expression of E2 regulated genes in indicated cell lines following a 16 hour treatment with DMSO, 10 nM raloxifene (Ral) or 4 nM fulvestrant (Fulv). Red= high expression; blue= low expression. **C,** CTG-based proliferation assays performed for indicated engineered MCF7 cell lines following a 6 day treatment with increasing concentrations of fulvestrant (upper) or 4-OHT (lower). Data normalized to DMSO control and each data point presented as mean ± SD. **D,** Sequence alignment highlighting cysteine at 530 position (shown in red) is only conserved in ER and not the other steroid nuclear hormone receptors. **E,** Structure of HB-5942, first-in-class covalent ERα antagonist. **F,** Mass spectrometry-based validation of covalent engagement of H3B-5942 with $ERα^{WT}$ (top panel) and $ERα^{Y537S}$ (third panel) LBDs. C530 was validated as the site of covalent engagement as binding was not observed with $ERα^{WT}$ and $ERα^{Y537S}$ LBDs bearing C530S mutation ($ERα^{C530S}$ (second panel) and $ERα^{C530S,\ Y537S}$ (bottom panel), respectively). **G,** X-ray structure of H3B-5942 demonstrating covalent engagement with C530 of $ERα^{Y537S}$ mutant receptor at 1.89 Å resolution.

Figure 2.

H3B-5942 induces an ERα conformational profile distinct from SERMs/SERDs. **A,** Western blot showing ERα expression following a 24 hour incubation with various doses of fulvestrant, 4-OHT, and H3B-5942 in MCF7 parental (MCF7-Parental) and PDX-ER$\alpha^{Y537S/WT}$ lines. GADPH served as loading control. **B,** Mammalian 2-hybrid assay was performed to monitor interaction of ERα^{WT}, ERα^{Y537S} and ERα^{D538G} with conformation selective peptide probes. Luciferase signal was measured after 24 hours of compound treatment at saturating concentrations (10 μM for all indicated compounds). Red indicates strong recruitment, blue indicates weak recruitment, and gray indicates average recruitment across all treatment conditions for each conformation-specific peptide. The peptide probes were clustered with UPGMA (Unweighted Pair Group Method with Arithmetic Mean) method and correlation distance measure. **C,** qPCR analysis of *PGR* expression in Ishikawa cells treated with various compounds for 24 hours at 3, 10, 30, 100 and 300 nM. Data presented as mean fold change ± SD relative to DMSO treatments. Data from a representative experiment are shown. **D**, CTG-based proliferation data for Ishikawa cells following 3 days of treatment with the indicated compounds at 3, 10, 30, 100 and 300 nM. Data presented as mean fold change ± SD relative to DMSO treatment. Data from a representative experiment is shown. **E,** IncuCyte-based 13-day time course analysis of confluence of Ishikawa cells following treatment with DMSO alone, 100 nM E2, 100 nM 4-OHT, 100 nM fulvestrant or 100 nM H3B-5942. Data presented as mean ± SEM (N=9). *p<0.05 versus vehicle control, **p<0.0001 versus vehicle control (two-sided t-test). Representative images of Ishikawa cells shown in right panel following 13 days of treatment with DMSO, 4-OHT, fulvestrant or H3B-5942.

Figure 3.

H3B-5942 is critically dependent on covalency for ERα antagonism. **A,** (Top) Structure of H3B-9224, saturated analog of HB-5942 lacking the internal Michael acceptor. (Bottom) Comparison of the co-crystal structures of $ER\alpha^{Y537S}$ ligand-binding domain bound to H3B-5942 (green) or H3B-9224 (cyan). The overlay shows that the pharmacophore binds in the same place, but the linker conformation is different. For H3B-5942, the linker projects towards C530 forming the covalent bond. In H3B-9224, the linker density is not well defined after the allylic nitrogen indicating conformational flexibility in that part of the ligand. **B,** Jump dilution experiment to evaluate reversibility of binding of estradiol and various inhibitors to $ER\alpha^{WT}$ and $ER\alpha^{Y537S}$. $ER\alpha^{WT}$ (His-TEV-ERα-C381S-C417S (307-554)) and $ER\alpha^{Y537S}$ (His-TEV-ERα-C381S-C417S-Y537S (307-554)) were incubated with an excess of ligands and incubated at room temperature for 5 hours to achieve binding equilibrium. After 5 hours, the binding mixture was diluted 20-fold and signal was determined using an excess of competing ^{3}H-estradiol using the hydroxyapatite binding assay in which the binding of ^{3}H-estradiol is only possible after dissociation of the pre-bound ligand. **C,** (Left panel) Representative plots showing dose-dependent suppression in *GREB1* (top) and *TFF1* (bottom) expression in $ER\alpha^{WT}$ (left) and $ER\alpha^{Y537S}$ (right) expressing MCF7 cells following a 6 day treatment with H3B-5942 (green solid) and H3B-9224 (green dotted), respectively. (Right panel) Table summarizing IC_{50} values from *GREB1* and *TFF1* expression analysis in $ER\alpha^{WT}$, $ER\alpha^{Y537S}$, $ER\alpha^{Y537N}$, $ER\alpha^{Y537C}$, and $ER\alpha^{D538G}$ overexpressing MCF7 lines following treatment with H3B-5942 and H3B-9224. Data shown from a representative experiment. **D,** (Left panel) Graphs showing a dose-dependent decrease in proliferation of $ER\alpha^{WT}$ and $ER\alpha^{Y537S}$ MCF7 overexpressing lines with or without C530S mutation in ERα following 6-day treatment with H3B-5942 (left) and H3B-9224 (right).

(Right panel) Table summarizing mean GI_{50} ± SD from $ER\alpha^{WT}$, $ER\alpha^{Y537S}$, $ER\alpha^{WT-C530S}$, and $ER\alpha^{Y537S-C530S}$ overexpressing MCF7 lines.

Figure 4.

H3B-5942 demonstrates potent ERα antagonist activity *in vitro* and *in vivo*. **A,** Graphs showing a dose-dependent decrease in *GREB1* expression in MCF7 lines engineered to overexpress $ER\alpha^{WT}$, $ER\alpha^{Y537S}$, $ER\alpha^{Y537N}$, $ER\alpha^{Y537C}$ and $ER\alpha^{D538G}$, and in the PDX-$ER\alpha^{Y537S/WT}$ cell line, following 6 day treatment with H3B-5942, 4-OHT, fulvestrant, and GDC-0810. All data points presented as mean ± SEM from a representative experiment. **B**, Table summarizing GI_{50} values for ERα+ (engineered MCF7 lines and PDX-$ER\alpha^{Y537S/WT}$) and ERα- (MDA-MB-231) cells lines treated with H3B-5942, 4-OHT, fulvestrant, and GDC-0810 for 6 days. All data presented as mean ± SEM from at least 3 biological replicates. **C,** Antitumor activity of H3B-5942 compared to tamoxifen and fulvestrant in the $ER\alpha^{Y537S/WT}$ ST941 PDX model. H3B-5942 was administered orally QD at 3, 10, 30, 100 and 200 mg/kg in mice bearing PDX tumors representing $ER\alpha^{Y537S/WT}$ breast cancer. Tamoxifen was dosed SC TIW at 1 mg/mouse whereas fulvestrant was dosed SC QW at 5 mg/mouse. Data represent the mean tumor volume ± SEM (N=6). * $p<0.05$, ** $p<0.001$ versus vehicle control (multiple unpaired t-tests with significance determined using the Holm-Sidak method). All doses and regimens were well tolerated. **D,** Gene expression analysis of ERα target genes *PGR* and *SGK3* in endpoint ST941 tumors from the study presented in panel **(C)**. Data presented as dot plot for 4 tumors/group normalized to *HK* with horizontal lines indicating mean normalized expression/group.

Figure 5.

H3B-5942 in combination with CDK4/6 inhibitors leads to enhanced potency and efficacy in breast cancer lines *in vitro*. **A**, To find synergistic drug combinations, a reference compound collection was profiled in dose-response +/- 1 µM H3B-5942 *in vitro* against the PDX-ER$\alpha^{Y537S/WT}$ line for 6 days. Results for all combinations were plotted as the fold standard deviation of the difference in the area under the curves. Inset shows the top 10% of the test, and results for the CDK4/6 inhibitors tested are summarized in the table. **B**, Combinations of H3B-5942 plus CDK4/6 inhibitors were confirmed as synergistic *in vitro* in MCF7 cells engineered to overexpress ERα^{WT}. H3B-5942 was tested in combination with palbociclib, ribociclib, and abemaciclib over the range of 2.5 µM to 25 pM for 6 days and then assessed for viability/proliferation (n=2). Data were normalized to untreated controls and to data at time zero (T0), where 100% and 0% equal uninhibited growth and stasis, respectively. Analysis of synergy used the Loewe Model, and the results were graphed in Combenefit software using the dose-response surface view of synergy/antagonism. **C-D,** Antitumor activity of H3B-5942 or 75 mg/kg palbociclib, as single agents or in combination, in the **(C)** MCF7 model and **(D)** ER$\alpha^{Y537S/WT}$ ST941 model. Data represent the mean tumor volume ± SEM (N=7 for H3B-5942 groups, N=8 for all other groups in the MCF7 study; N=6 for all groups in the ST941 study). *p<0.001, **p<0.0001 versus vehicle control (multiple unpaired t-tests with significance determined using the Holm-Sidak method). All doses and regimens were well tolerated.

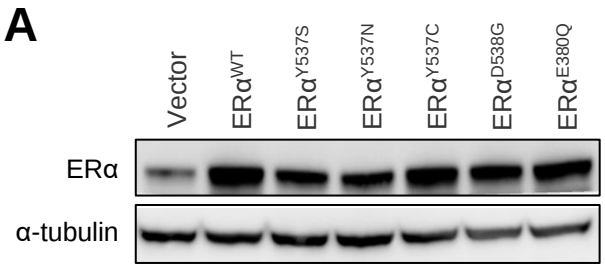

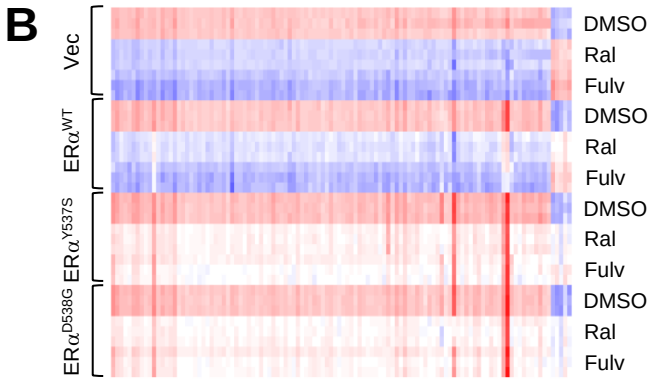

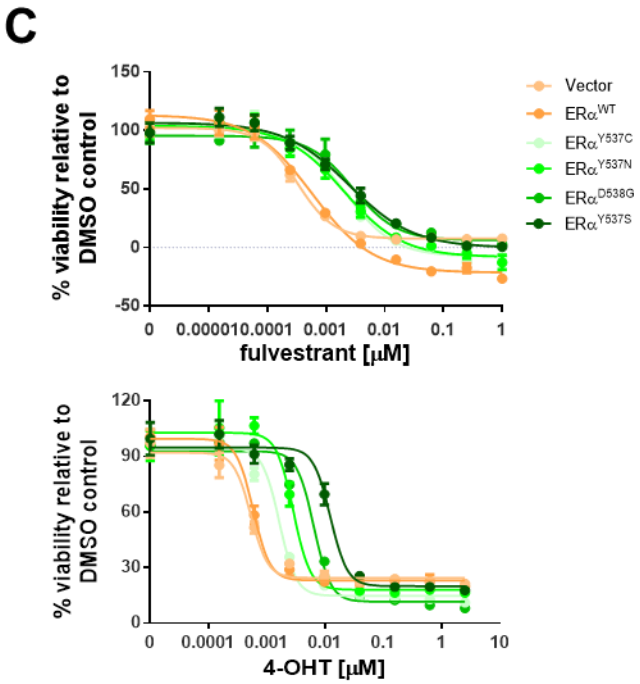

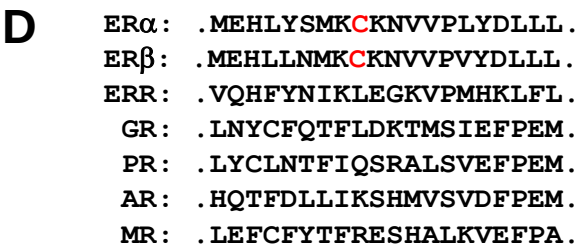

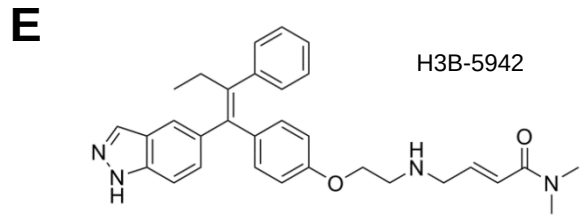

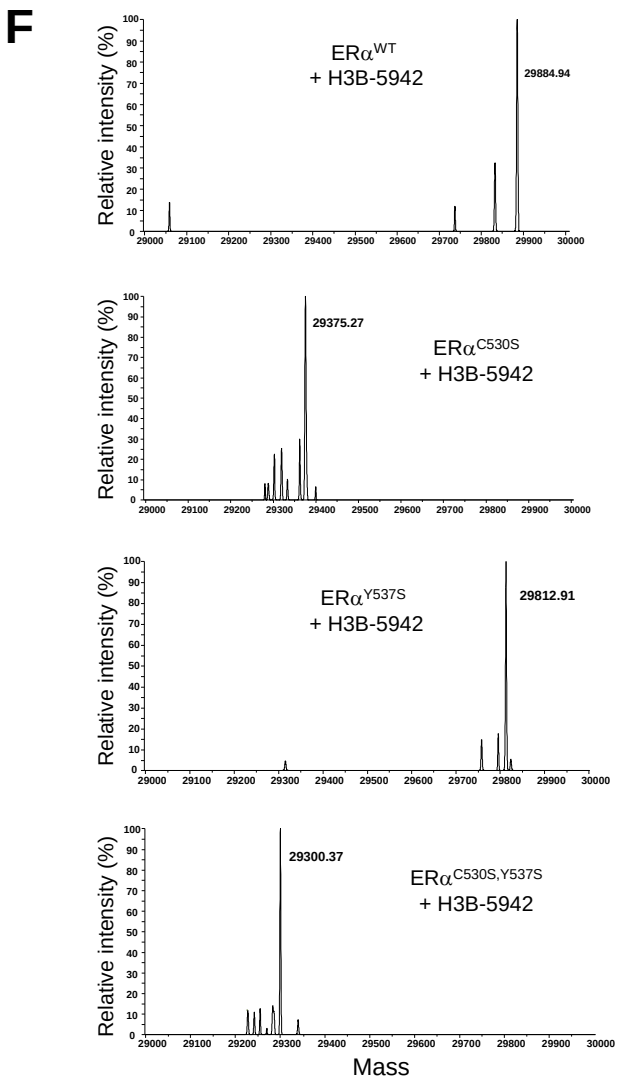

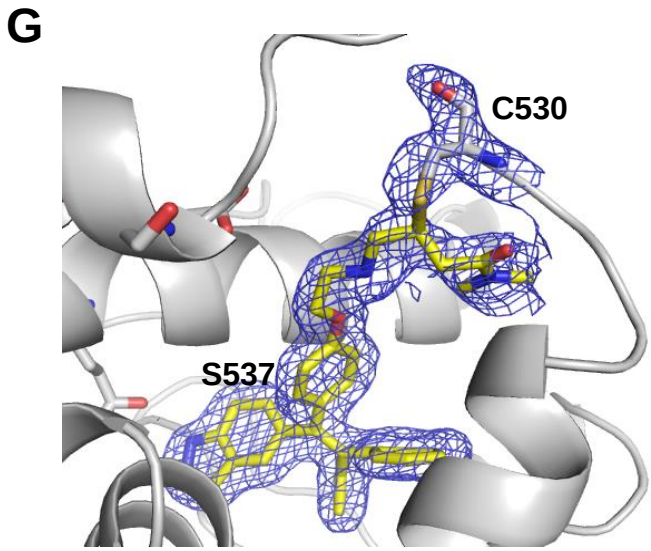

Figure 1

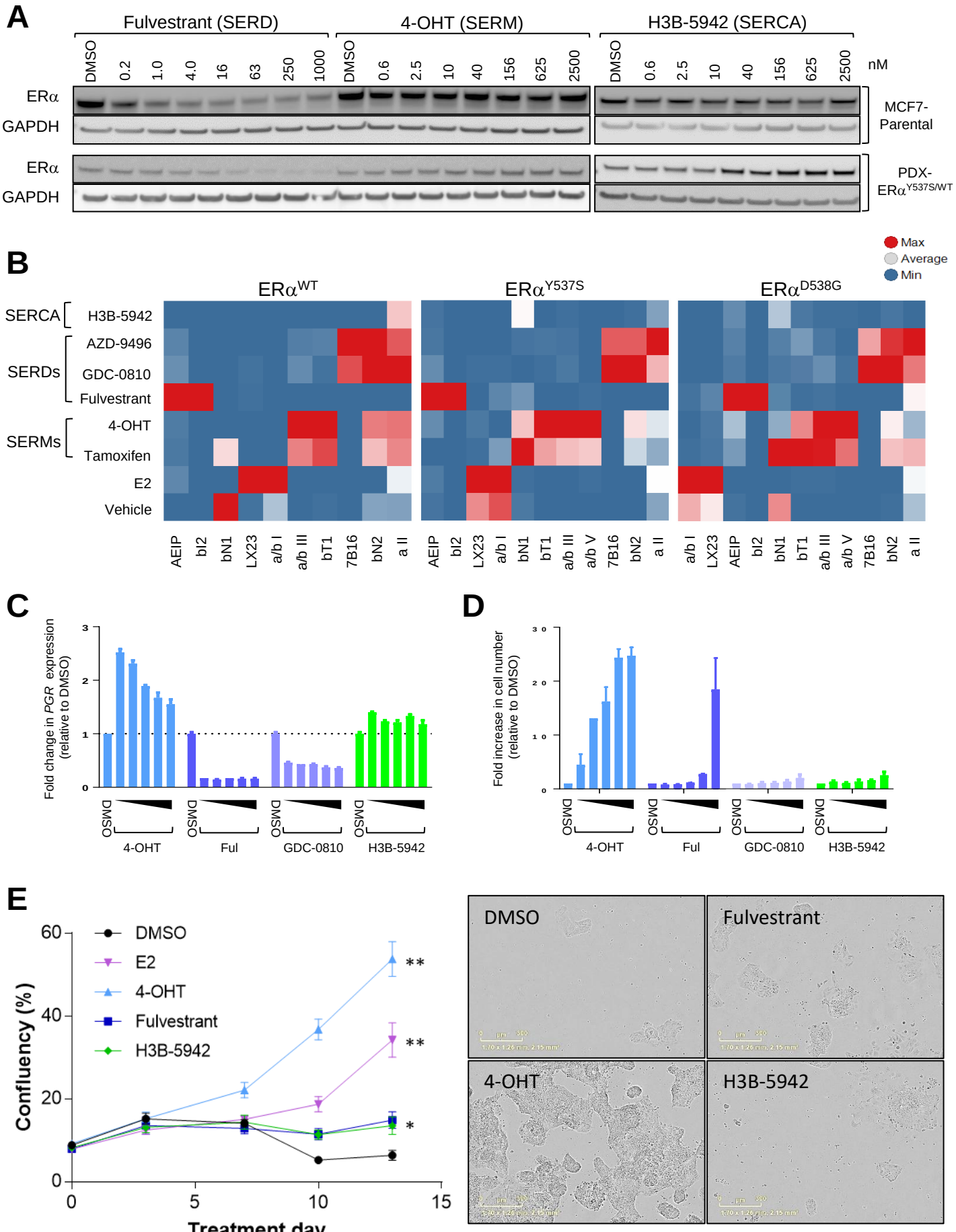

Figure 2

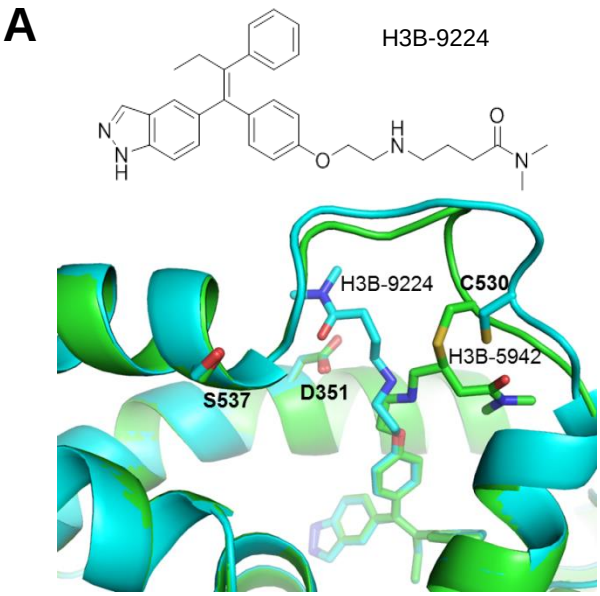

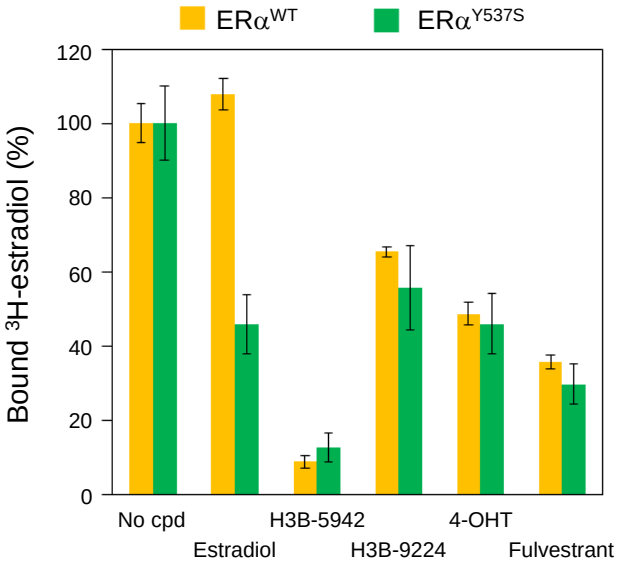

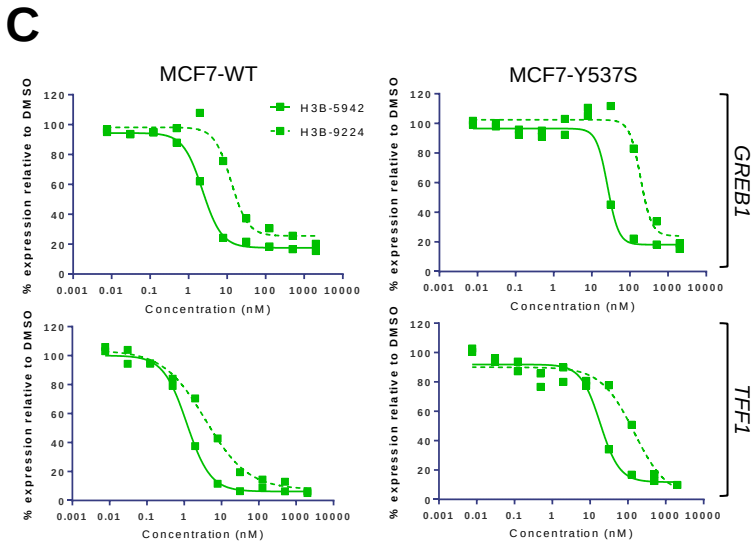

GREB1 (IC_{50}, nM)

Compound	WT	Y537S	Y537N	Y537C	D538G
H3B-5942	2.74	29.38	8.14	12.19	24.87
H3B-9224	17.8	297.21	103.9	165.4	85.72

TFF1 (IC_{50}, nM)

Compound	WT	Y537S	Y537N	Y537C	D538G
H3B-5942	1.3	19.4	6.1	9.5	4.0
H3B-9224	5.0	119.5	31.5	106.6	16.4

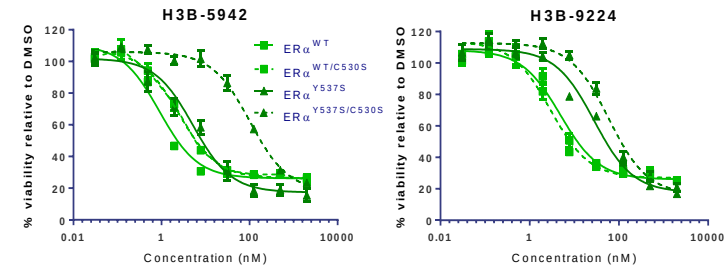

Viability (GI_{50}, nM)

Compound	WT	WT-C530S	Y537S	Y537S-C530S
H3B-5942	1.3 ± 0.4	4.2 ± 1.3	8.3 ± 1.7	193 ± 45.7
H3B-9224	5.1 ± 2.3	4.4 ± 1.4	43.6 ± 10.3	77.1 ± 21.5

Figure 3

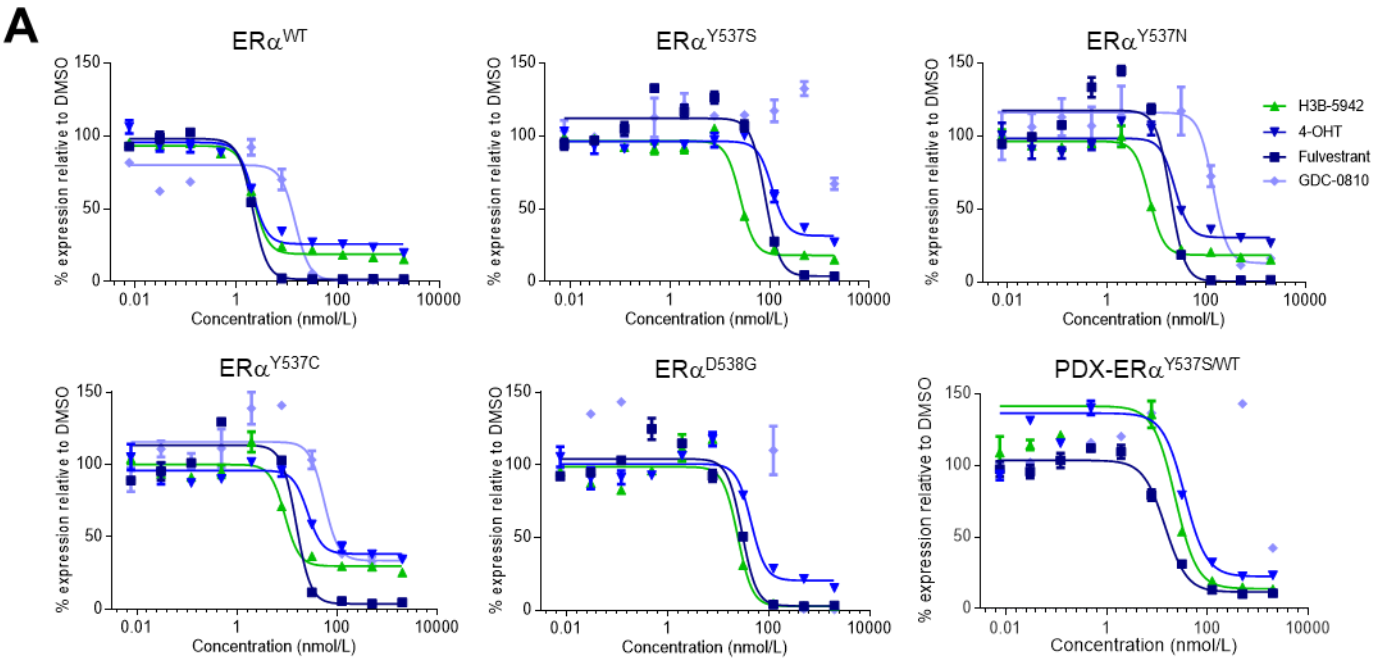

B

Viability- CTG-Glo, GI_{50} (nM)

Compound	MCF7 ($ER\alpha^{WT}$)	MCF7 ($ER\alpha^{Y537S}$)	MCF7 ($ER\alpha^{Y537N}$)	MCF7 ($ER\alpha^{Y537C}$)	MCF7 ($ER\alpha^{D538G}$)	PDx ($ER\alpha^{Y537S/WT}$)	MDA-MB-231 (ERα-negative)
H3B-5942	1.2 ± 0.6	6.5 ± 2.5	3.0 ± 0.8	2.5 ± 1.0	8.1 ± 4.3	6.5 ± 2.0	> 1000
4-OHT	1.6 ± 0.5	17.9 ± 7.2	6.5 ± 0.8	5.1 ± 1.0	12.9 ± 5.1	13.5 ± 3.2	> 1000
Fulvestrant	0.9 ± 0.2	2.9 ± 0.6	2.6 ± 0.3	2.9 ± 0.5	4.1 ± 1.5	10.4 ± 2.4	> 1000
GDC-0810	11.6 ± 1.8	126.4 ± 54.8	59.6 ± 11.4	34.2 ± 5.6	73.1 ± 37.3	273.8 ± 29.5	> 1000

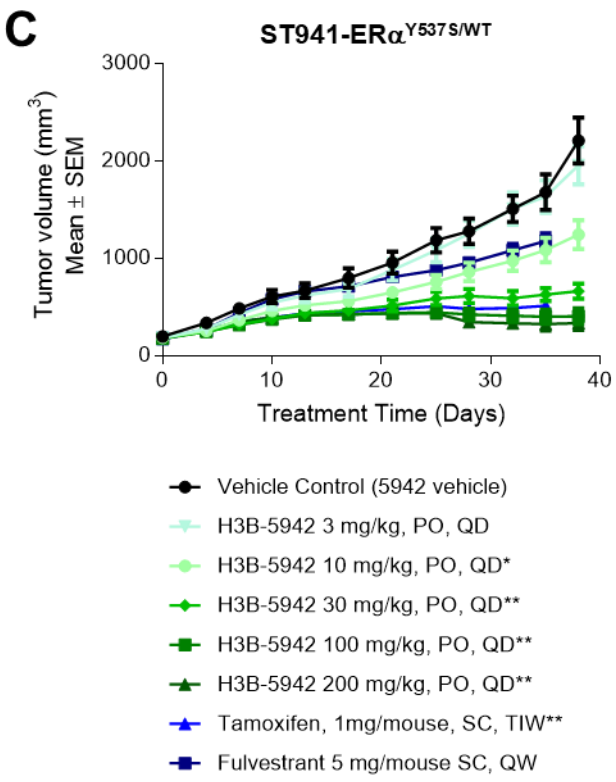

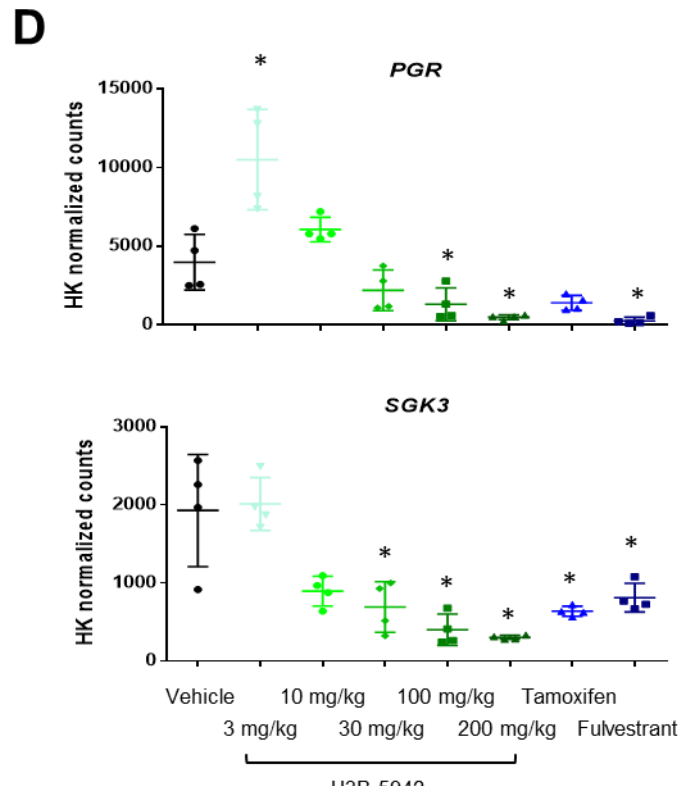

Figure 4

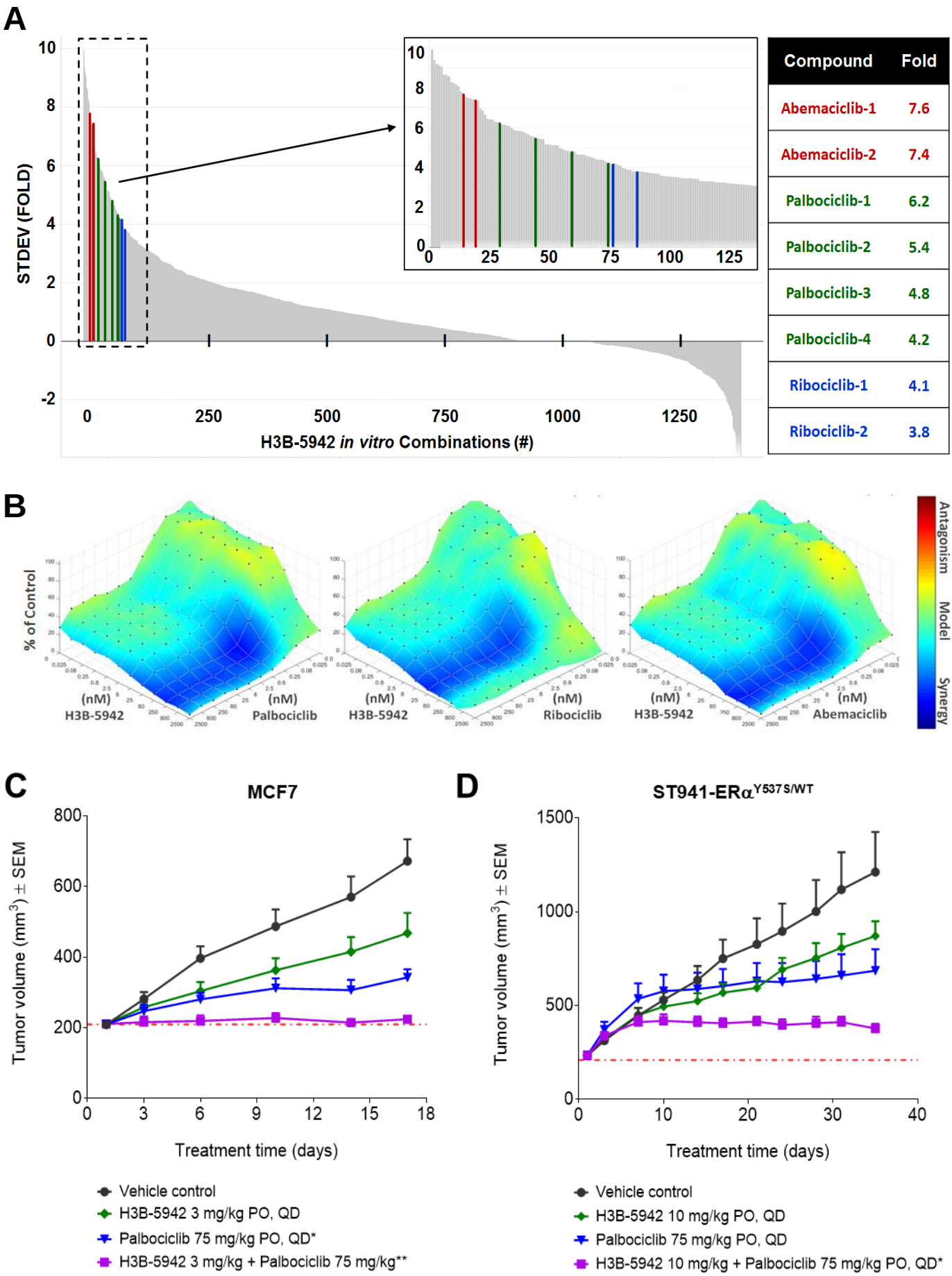

Figure 5

AACR American Association for Cancer Research

CANCER DISCOVERY

Discovery of Selective Estrogen Receptor Covalent Antagonists (SERCAs) for the treatment of ERa(WT) and ERa(MUT) breast cancer.

Xiaoling Puyang, Craig Furman, Guo Zhu Zheng, et al.

Cancer Discov Published OnlineFirst July 10, 2018.